From spheres to circular cylinders: non-axisymmetric transitions in the flow past rings

By G. J. SHEARD, M. C. THOMPSON
AND K. HOURIGAN

Fluids Laboratory for Aeronautical and Industrial Research (FLAIR), Department of
Mechanical Engineering, Monash University, Melbourne, Victoria 3800, Australia

Non-axisymmetric simulations verify and extend the results from a previous linear Floquet stability analysis of the wakes of rings. The wakes corresponding to the saturated state of each predicted non-axisymmetric instability mode over the entire aspect ratio range are successfully computed, and isosurface plots are presented elucidating the vortical wake structures. The existence of three non-axisymmetric flow regimes (Modes I, II and III) for the flow past rings with aspect ratios $Ar \lesssim 3.9$ is verified, as is the existence of non-axisymmetric instabilities of vortex streets in the flow past rings with $Ar \gtrsim 3.9$. Wakes are computed which correspond to the Mode A and B instabilities found in the flow past a circular cylinder, and a wake is computed which develops from a subharmonic Mode C instability. This wake features an azimuthal wavelength of approximately 1.7 ring cross-section diameters, which is between the azimuthal wavelengths of the Mode A and B instabilities. This mode cannot occur, at least in a pure state, in the flow past a circular cylinder.

Nonlinear transition characteristics are predicted by evaluating coefficients of the truncated Landau equation, and transition hysteresis is verified by studying the mode amplitude variation with Reynolds number in the vicinity of the transitions. The regular Mode I and Mode III transitions are found to occur through supercritical and subcritical bifurcations, respectively, and the secondary Hopf bifurcations to these transitions, as well as the Mode II Hopf transition, are found to be supercritical. We verify that the Mode A and Mode B transitions are subcritical and supercritical, respectively, and we determine that the nature of the Mode C transition is dependent on aspect ratio. Landau constants are evaluated for the Hopf transitions throughout the aspect ratio range studied.

1. Introduction

The route to turbulence associated with an increase in Reynolds number in the flow past bluff bodies has been the subject of a significant body of research over many years. The flows past simple geometries such as the sphere (Taneda 1956; Magarvey & Bishop 1961*b*; Johnson & Patel 1999; Tomboulides & Orszag 2000), the circular cylinder (Williamson 1988*a*, 1996), and the rectangular cylinder (Hourigan, Thompson & Tan 2001; Mills, Sheridan & Hourigan 2002, 2003) have all been studied to gain an understanding of the intermediate flow states and the transitions which can be found between the steady attached laminar flows at low Reynolds numbers

(typically $Re < 5$ for the flow past a circular cylinder) and the chaotic turbulent flows at high Reynolds numbers (typically $Re > 500$ for the flow past a circular cylinder). The remnants of these transitions often persist even in fully developed turbulent flow. For example, Strouhal shedding and three-dimensional structures with a spanwise wavelength consistent with the Mode B instability persist up to high Reynolds numbers ($Re \approx 10\,000$) for the flow past a circular cylinder (Wu *et al.* 1996).

The intermediate wake states observed are due either to linear instabilities of the flow field, such as the three-dimensional instabilities of the vortex street in the flow past a circular cylinder (Barkley & Henderson 1996), or to global effects such as oblique shedding modes (Williamson 1988*a*, 1989).

The separation of the boundary layer in the flow past a sphere and a circular cylinder has been observed to occur prior to the occurrence of linear instability modes in these flows. As the transition to separated flow marks the beginning of the formation of a recirculation bubble behind a bluff body, which in turn becomes unstable to the various modes studied here, it is of underlying importance. Tomboulides & Orszag (2000) found the transition to separated flow to occur in the flow past a sphere at $Re = 21$, and the cylinder transition at $Re = 6$ was predicted by Noack & Eckelmann (1994).

The linear instabilities that arise in the wake behind a sphere have been studied by Natarajan & Acrivos (1993). They predicted that the wake behind the axisymmetric sphere and disk undergoes a regular (steady–steady) non-axisymmetric transition, followed by a Hopf (unsteady) transition at higher Reynolds numbers. Both these transition modes have $m = 1$ azimuthal symmetry (only one wavelength of the unstable mode around the circumference of the body). Both experimental observations (Magarvey & Bishop 1961*a,b*; Magarvey & MacLatchy 1965), and non-axisymmetric numerical simulations (Johnson & Patel 1999; Tomboulides & Orszag 2000; Thompson, Leweke & Provansal 2001*a*) support these findings for the flow past a sphere, as well as the predicted critical Reynolds number for the initial regular transition. The structure of the flow past a sphere following the initial non-axisymmetric transition is characterized by a transverse shift of the recirculation bubble behind the sphere away from the axis, and the development of a counter-rotating pair of streamwise vortical tails stretching far downstream. These tails are located either side of a plane of symmetry along the axis (Johnson & Patel 1999). Just prior to the Hopf bifurcation, a deformation of the twin vorticity tails occurs as they are drawn closer together (Thompson *et al.* 2001*a*) at the rear of the recirculation bubble. After the secondary transition, the bubble becomes unstable and sheds vorticity into the wake, forming hairpin-shaped vortices shedding on opposite sides of the axis every half-period (Tomboulides & Orszag 2000). A plane of symmetry in the wake is maintained following the secondary Hopf transition (Mittal 1999) until $Re \approx 375$. In order to study geometric effects on bluff body wake transition, the wakes from rings aligned normal to the direction of flow are studied. Figures 1 and 2 show a schematic representation of the ring system. The aspect ratio of the rings is given by the relationship

$$Ar \equiv \frac{D}{d} \qquad (1.1)$$

where D is the mean ring diameter and d is the diameter of the cross-section of the ring. By varying the single geometric parameter Ar, a uniform axisymmetric body is described which varies from a sphere at $Ar = 0$ to a circular cylinder (local to the cross-section of the ring) in the limit $Ar \rightarrow \infty$. The present study defines a Reynolds
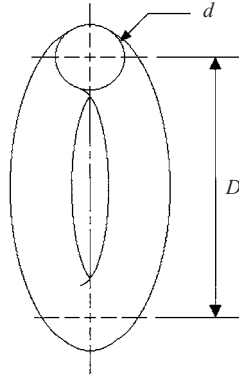
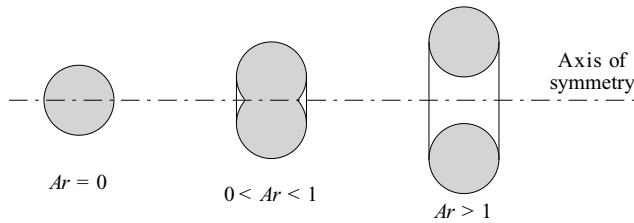FIGURE 1. Dimensions of the ring. The aspect ratio is given by $Ar = D/d$.

FIGURE 2. Cross-section views showing the distinct geometries that are described by the aspect ratio parameter. A sphere with $Ar = 0$ is shown at the left, a closed ring with $Ar \leqslant 1$ is shown at the centre, and an open ring with $Ar > 1$ is shown at the right.

number

$$Re \equiv \frac{Ud}{\nu}, \tag{1.2}$$

where U is the free-stream velocity and ν is the kinematic viscosity of the fluid.

Monson (1983) studied the drag and vortex shedding behind rings of various diameters falling through a fluid. A variety of shedding patterns were observed and, as the minor cross-section of the ring became smaller with respect to the outer diameter of the ring, the shedding patterns and drag characteristics approached those observed behind the straight circular cylinder. This characteristic of the ring geometry partially motivated an experimental study by Leweke & Provansal (1995), who used rings with large aspect ratios to approximate the wake behind a circular cylinder, but without the end effects that are difficult to avoid with straight circular cylinders experimentally. Strouhal–Reynolds number profiles were presented for various rings which showed the discontinuities associated with the onset of non-axisymmetric instabilities in the wake, but no flow visualization of these modes was provided. For smaller aspect ratios ($Ar \lesssim 6$), Bearman & Takamoto (1988) observed the wake behaviour of the rings to more closely resemble the wakes behind a sphere or disk than the circular cylinder. The critical aspect ratio at which the flow past a ring switches from a circular-cylinder-type vortex shedding to a sphere-type hairpin wake was suggested by Monson (1983) to occur at $Ar \approx 4.5$. The recent well-resolved numerical study of Sheard, Thompson & Hourigan (2001) predicts this switch to occur at an aspect ratio of $Ar \approx 3.9$.

A study of non-axisymmetric instability modes of the wakes of rings by application of a linear stability analysis scheme was made by Sheard et al. (2001, 2003). The

lengthscale for their Reynolds number calculations was the diameter of the ring cross-section, d, consistent with the accepted sphere and circular cylinder lengthscales widely used in the literature. The analysis predicted modes of vortex shedding analogous to both the Mode A and Mode B transition modes identified in the flow past the circular cylinder experimentally (Williamson 1988b), and by numerical stability analysis (Barkley & Henderson 1996; Thompson, Leweke & Williamson 2001b). The critical Reynolds numbers for the Mode A and Mode B transitions in the wakes of rings varied over the ranges $188 \lesssim Re \lesssim 200$ and $258 \lesssim Re \lesssim 300$, respectively. The azimuthal wavelengths for the modes were found to be approximately $3.9d$ for the Mode A instability, and $0.8d$ for the Mode B instability, in good agreement with numerical stability analysis of the flow past a circular cylinder (Barkley & Henderson 1996).

Evidence of a third non-axisymmetric instability was also found by Sheard *et al.* (2001, 2003). A real subharmonic transition mode was predicted to be unstable for azimuthal wavelengths $1.6d < \lambda < 1.7d$. These previous studies employed a power method for determining the Floquet multipliers of the instability modes. As the power method excludes the imaginary component of the computed Floquet multipliers, it is impossible to distinguish travelling-wave and standing-wave modes resulting from a complex-conjugate-pair Floquet mode. Before briefly revisiting the properties of the intermediate-wavelength mode predicted in these previous works, it is necessary to discuss some recent stability studies of the flow past a square-section cylinder.

A stability analysis employing the power method was applied to the flow past a square-section cylinder by Robichaux, Balachandar & Vanka (1999). They predicted a subharmonic mode (Mode S) of a spanwise wavelength comparable (when scaling with the diagonal dimension of the square cylinder) to the intermediate-wavelength mode predicted in the flow past rings. The subharmonic nature of the mode they found was assumed, as the perturbation field of the instability mode appeared to alternate in sign each period. Recent analysis by Blackburn & Lopez (2003) employed a more general method for determining the stability that included the imaginary component of the Floquet mode. Applying this method to the same square cylinder problem attempted by Robichaux *et al.* (1999), they found that Mode S was in fact a quasi-periodic mode, which consisted of a complex-conjugate-pair Floquet mode. The imaginary component of the mode was small compared to the (negative) real component, which explained why the mode was incorrectly identified as a subharmonic mode by Robichaux *et al.* (1999). Based on this recent square cylinder study, Blackburn & Lopez (2003) proposed the following bifurcation scenario for the time-periodic wakes of bluff bodies with a reflective symmetry about the wake centreline: a real short-wavelength mode (Mode B), a real long-wavelength mode (Mode A), and an intermediate-wavelength quasi-periodic mode (Mode QP or Mode S). This scenario is identical to the bifurcation scenario for the flow past a circular cylinder (Barkley & Henderson 1996), which possesses the same reflective symmetry properties.

A natural bifurcation from this scenario is to break the reflective symmetry of the wake. The placement of a trip-wire in the flow past a circular cylinder has been shown to introduce an intermediate-wavelength mode that displays subharmonic properties (Zhang *et al.* 1995). Their numerically predicted instability mode (Mode C) was most unstable for spanwise wavelengths of approximately $1.6d$, similar to the wavelength of the subharmonic Mode C instability in the flow past rings. It is possible that the bifurcation scenario for periodic wakes of bluff bodies lacking reflective symmetry may comprise real Modes A and B, and a real subharmonic Mode C. The predicted

dominance of the Mode C instability as the loss of reflective symmetry in the flow past rings becomes more pronounced with decreasing aspect ratio (Sheard *et al.* 2003) supports this conjecture.

Finally, we will briefly discuss the evidence that leads to the conclusion that the intermediate-wavelength instability in the flow past a ring is subharmonic, and not the result of a complex-conjugate-pair Floquet mode. A subharmonic mode (bifurcation through $\mu = -1$) has the unique property that the mode alternates in sign each period. The predicted Mode C instability produced a perturbation field that satisfied this behaviour, and in fact summing two perturbation fields exactly one base flow period apart produced a zero-perturbation velocity field to the limit of numerical precision. The Mode C instability also produced a convergent Floquet multiplier, which implies that no imaginary components were present to introduce incommensurate frequencies. Hence, Mode C is a genuine subharmonic mode.

Rings with smaller aspect ratios have been shown to exhibit wakes vastly different to the straight circular cylinder (Roshko 1953). He observed a similar decrease in frequency between the flow past rings and the flow past a circular cylinder to that quantified by Leweke & Provansal (1995). Furthermore, he observed a significant change in the Strouhal–Reynolds number profiles for much smaller rings. The aspect ratios at which this change occurred were smaller than those studied by Leweke & Provansal (1995); however, dye visualizations by Monson (1983) support the finding of Roshko (1953).

The tori with smaller aspect ratios studied by Monson (1983) gave an indication that a transition to an unsteady mode may occur, resulting in a wake similar to the hairpin shedding observed behind the sphere (Tomboulides & Orszag 2000; Johnson & Patel 1999). Stability analysis of the flow past rings with small aspect ratios ($Ar < 4$) by Sheard *et al.* (2001, 2003) has shown that the transition modes of the sphere are in fact observed for a variety of rings in the aspect ratio range $0 \leqslant Ar < 1.6$. Three distinct transition modes (Mode I, Mode II and Mode III) have been identified over the aspect ratio ranges $0 \leqslant Ar < 1.6$, $1.6 \leqslant Ar \leqslant 1.7$ and $1.7 < Ar \lesssim 3.9$, respectively.

The Mode I regime (which includes the sphere) is predicted to undergo a regular non-axisymmetric transition, which is followed by a Hopf transition at higher Reynolds numbers. The Mode I instability is predicted to occur at Reynolds numbers decreasing from $Re = 211$ at $Ar = 0$ to $Re = 72.6$ at $Ar = 1.4$ (Sheard *et al.* 2003).

The Mode II regime is predicted to comprise a curious spontaneous non-axisymmetric Hopf transition. Regular transition modes were identified in the Mode II regime; however, they remain absolutely stable for all Reynolds numbers.

The Mode III regime is predicted to be similar to the Mode I regime, with a regular non-axisymmetric transition being followed at higher Reynolds numbers by a Hopf transition.

It is interesting to compare the dye visualization experiments of Monson (1983) with the numerically predicted three-dimensional transition scenarios presented here. Despite the minor differences in system configuration (e.g. in the experiments the rings were allowed to fall freely through the fluid, lacking any constraint in movement), the flow past rings with large aspect ratios was found to exhibit cylinder-style vortex shedding, whereas the flow past rings with small aspect ratios (high solidity) was found to undergo a regular non-axisymmetric transition prior to a Hopf transition. For example, Monson observed a periodic non-axisymmetric wake for a ring with $Ar \approx 2.6$ at $Re = 115$. Interpolating the critical Reynolds number profiles from Sheard *et al.* (2003) shows that the Hopf bifurcation would occur for Reynolds numbers $100 \lesssim Re \lesssim 105$, in reasonable agreement with the experimental observations.

This work aims to verify the existence of the non-axisymmetric transition modes predicted previously, through non-axisymmetric computations of the three-dimensional wakes. The nonlinear transition properties will be predicted by fitting coefficients to the truncated Landau equation, described in §2. Particular attention will be given to the hysteretic properties of the transition modes. The predictions of the Landau model will be verified by studying the variation in amplitude of the non-axisymmetric modes in the vicinity of the transitions to determine if bi-stable states exist.

Properties of the Hopf transition for rings will be investigated by determining the values of constants derived from the Landau model that pertain to the Strouhal frequency shift through saturation, and the diffusivity properties of the transitions.

2. Transition behaviour

The Landau model provides a means for studying the nonlinear behaviour near the transition Reynolds number. It has been used widely in describing and classifying bluff-body wake transitions: for example, the circular-cylinder wake Hopf bifurcation (Provansal, Mathis & Boyer 1987; Dušek, Fraunié & Le Gal 1994; Zielinska & Wesfreid 1995); the circular cylinder Mode A and B transitions (Henderson 1997); and the sphere wake transitions (Ghidersa & Dušek 2000; Thompson *et al.* 2001*a*; Provansal & Ormières 1998).

Landau & Lifshitz (1976) proposed a model to describe the growth and saturation of the perturbation post-transition. The governing equation is

$$\frac{\mathrm{d}A}{\mathrm{d}t} = (\sigma + \mathrm{i}\omega)A - l(1 + \mathrm{i}c)|A|^2 A + \dots, \tag{2.1}$$

where $A(t)$ is a complex variable representing the mode amplitude. A description of this equation, and its application to stability analysis, is provided in Provansal *et al.* (1987). Here, we review briefly the characteristics of the model and the method of its application pertinent to the present study.

The complex variable $A(t)$ represents the amplitude of the perturbation mode from the base flow. The right-hand side of the equation gives the first two non-zero terms of a series expansion. Provided l is positive, these first two terms should provide a good description of the nonlinear behaviour in the neighbourhood of the transition, since the saturated amplitude should still be small. This is not true if l is negative; in that case, the cubic term accelerates the growth of the perturbation and quintic or even higher-order terms are required to describe saturation of the mode. Thus, the sign of l plays an important role in classifying the transition. Positive l means the transition is supercritical (non-hysteretic), while negative l means it is subcritical (hysteretic). The parameter σ is the linear growth rate of the perturbation, and at the transition point its value changes from negative to positive. Also, ω is the angular oscillation frequency during the linear growth phase, which is non-zero for a Hopf bifurcation. The parameter c is called the Landau constant. It is a non-dimensional quantity (unlike l) and hence does not depend on the position in the wake where $A(t)$ is measured. It modifies the oscillation frequency at saturation, and in addition, its size and magnitude determine global behaviour in related flow systems such as wake behaviour under external oscillatory forcing (Le Gal, Nadim & Thompson 2001).

The usual way to manipulate the Landau equation (i.e. Dušek *et al.* 1994) is to write the complex amplitude variable as

$$A = \rho \exp(\mathrm{i}\Phi). \tag{2.2}$$

Here, $\rho = |A|$ is a real variable describing the mode amplitude, and Φ is a real variable providing the phase of the mode. The Landau equation can then be split into real and imaginary parts:

$$\frac{\mathrm{d}\log(\rho)}{\mathrm{d}t} = \sigma - l\rho^2 + \ldots, \tag{2.3}$$

$$\frac{\mathrm{d}\Phi}{\mathrm{d}t} = \omega - lc\rho^2 + \ldots. \tag{2.4}$$

Using equation (2.3) and noting that at saturation the (real) amplitude will not change in time, gives $\rho_{sat}^2 = \sigma/l$. In addition, since σ is necessarily proportional to the Reynolds number increment above the critical Reynolds number in the neighbourhood of a simple transition, the energy in the mode (proportional to ρ^2) varies as $Re - Re_c$, where Re_c is the critical Reynolds number. This behaviour has been verified numerically (e.g. Dušek *et al.* 1994) and experimentally (e.g. Ormières & Provansal 1999) for different supercritical wake transitions. The equation for the phase (2.4) also provides useful information. If the flow reaches a periodic state at saturation, $\mathrm{d}\Phi/\mathrm{d}t$ becomes the constant angular frequency of oscillation (ω_{sat}). It takes the value $\omega_{sat} = \omega - lc\rho_{sat}^2 = (\omega + \sigma c)$. Hence, σc determines the shift from the oscillation frequency in the linear regime, as the flow saturates.

Provansal *et al.* (1987) showed that the viscous diffusion timescale (d^2/ν) is proportional to $(Re - Re_c)/\sigma$. Grouping these terms allows the constant of proportionality to be expressed:

$$\text{Landau diffusivity constant} = \frac{Re - Re_c}{\sigma} \times \frac{\nu}{d^2}. \tag{2.5}$$

This constant has been evaluated from experimental measurements for the Hopf transiton of a circular cylinder wake by Provansal *et al.* (1987). They found the value of the constant to be approximately 5. Using the data presented in Thompson *et al.* (2001*a*), the Landau diffusivity constant may be computed for the Hopf transition of a sphere wake. At $Re = 280$ ($Re - Re_c \approx 7.8$), they predicted the Hopf transition to grow with $\sigma \approx 0.015$, and this yields a Landau diffusivity constant of approximately 1.86.

For regular (i.e. steady–steady) transitions, only the real component of the amplitude A need be considered, and hence equation (2.3) is applied. For transitions involving time-dependent flows, the phase of the amplitude is considered by applying equation (2.4).

Given equation (2.3), it is possible to determine the real parameters in the model from numerical computations by plotting $\mathrm{d}\log|A|/\mathrm{d}t$ against $|A|^2$. The y-intercept gives the linear growth rate σ and the gradient for small amplitudes near to the y-axis yields $-l$. For the truncated cubic Landau model to describe the transition well, equation (2.3) indicates the plot should be linear. Plotted this way, the time trajectory of the transition should start at the y-axis, and finish on the x-axis if the flow reaches a periodic or steady asymptotic state. If the slope of the curve is positive at the y-axis, the transition is subcritical and at least quintic terms are required in the Landau equation to describe the saturation process with any accuracy. In the vicinity of the transition, it is possible to determine the Landau constant by measuring the oscillation frequency of the perturbation in the linear regime and at saturation, and by rearranging equation (2.4) to form equation (2.6):

$$c = \frac{\omega_{sat} - \omega}{\sigma}. \tag{2.6}$$

From a numerical point of view, the derivative $(\mathrm{d}\log|A|/\mathrm{d}t)$ can be accurately estimated using finite differences. For transitions to a time-dependent final state, the signal at small times is initially sinusoidal multiplied by an exponential growth factor. At larger times, as the flow saturates, the amplitude envelope asymptotes to a constant width and the sinusoidal oscillation frequency adjusts slightly according to equation (2.4). Thus, in the more complicated case of transition to a time-dependent final state, the derivative can be estimated by finite differences of the envelope of the amplitude of the unstable mode.

To proceed further, the amplitude variable A needs to be specified. Previous studies have taken different approaches. For example, Dušek *et al.* (1994) and Thompson *et al.* (2001*a*) used the transverse velocity component at a fixed point on the centerline of the circular cylinder wake. Zielinska & Wesfreid (1995) instead used the maximum transverse velocity component on the centreline. The position at which this occurs varies with Reynolds number. Henderson (1997) used the L_2 norm of the spanwise velocity component for examining two-dimensional to three-dimensional transitions for the flow past a circular cylinder. However, because the numerical domain was necessarily truncated downstream before the mode amplitude decayed to zero, this also was not a unique global measure. For the analysis presented in this paper, the L_2 norm method, as described in Henderson (1997) and Thompson *et al.* (2001*a*), is employed. As the transitions studied in this paper are non-axisymmetric transitions, an L_2 norm is computed based on an integration of the azimuthal velocity component of the wake, as follows:

$$|A| \equiv \left[\Psi_{\text{cylinder}} \int_V w^2 \, \mathrm{d}V \right]^{1/2}, \qquad (2.7)$$

where $|A|$ is the amplitude of the mode in question, Ψ_{cylinder} is a normalizing coefficient set to unity for simplicity, V is the volume of the computational domain, and w is the azimuthal component of the velocity field.

For the regular transitions in the Mode I and Mode III regimes, and the vortex shedding transitions, the modes evolved from $|A| \approx 0$, and thus $|A|$ could be directly employed to determine the coefficients of the Landau model. To determine the Landau model coefficients for the time-dependent wakes that evolved from the Hopf transitions in the regimes of Modes I, II and III, the envelope of $|A|$ was captured.

Non-axisymmetric simulations are performed by employing randomly perturbed axisymmetric flow fields as an initial condition. The velocity perturbation had an amplitude of the order 10^{-4} of the mean flow. The flow fields were then evolved to saturation, and the time history of the amplitude evolution was recorded for post-processing.

3. Numerical method

A spectral-element method was used for the numerical simulations in this investigation. The numerical scheme is identical to the scheme employed by Thompson *et al.* (2001*a*) for the flow past a sphere, and follows closely the numerical scheme developed by Tomboulides & Orszag (2000). The method employs high-order tensor-product Lagrangian polynomials as the shape functions within each element. The node points of the Lagrangian polynomials correspond to the Gauss–Legendre–Lobatto quadrature points, allowing accurate and efficient integration over each element. For non-axisymmetric computations, a Fourier expansion of the velocity and pressure fields was employed in the azimuthal direction.

The numerical spectral-element software used here has been validated previously and employed successfully by Thompson *et al.* (2001*a*) for the flow past a sphere, and by Sheard *et al.* (2001, 2002, 2003) for the flow past rings. The resolution of the meshes constructed to model the ring geometries are consistent with similar numerical studies of both the sphere (Tomboulides & Orszag 2000; Thompson *et al.* 2001*a*) and the circular cylinder (Barkley & Henderson 1996; Henderson 1997). Upstream of the circular ring cross-section, and on the side boundary, a uniform-velocity inlet boundary is imposed. At the surface of the ring, a zero-velocity boundary condition is imposed, and at the axis, a zero-normal-velocity condition is imposed. At the downstream outlet, a zero normal velocity gradient is imposed.

Grid resolution studies (Sheard *et al.* 2001, 2002, 2003) determined the domain size, the number of mesh elements, and the required number of nodes per element to resolve flow field characteristics to within 1%. The meshes typically consisted of 380 to 400 macro elements, with 64 (8×8) nodes per element. To properly resolve the velocity field for $Re \gtrsim 300$, elements with 9×9 nodes per element were employed. The inlet length, transverse length, and outlet length were 15, 30 and 25 ring cross-section diameters, respectively.

4. Results I: small aspect ratios ($0 \leqslant Ar \lesssim 3.9$)

Here results are presented to illustrate the non-axisymmetric vortical structure and nonlinear transition characteristics of the wakes of rings with small aspect ratios. Aspect ratios were selected to isolate each of the three non-axisymmetric transition modes identified in previous work. The Mode I regime covers a wide aspect ratio range $0 \leqslant Ar < 1.6$, spanning the change in topology as the sphere transforms to a ring with a hole. Thus two aspect ratios, $Ar = 0.6$ and 1.2, are considered. For the Mode II regime $Ar = 1.6$ is studied. $Ar = 2.0$ and $Ar = 3.0$ are employed to represent the Mode III regime.

The nonlinear behaviour of the non-axisymmetric transition modes for rings with aspect ratios $Ar < 4$ is investigated in the following subsections. As described previously, the Landau equation is assumed to model the growth of non-axisymmetric transients in the flow past rings at Reynolds numbers near to the transition point. The coefficients of the Landau model are determined for each mode, and where applicable comparisons are drawn to previous work on sphere wake stability (Thompson *et al.* 2001*a*), (linear) ring wake stability Sheard *et al.* (2003), and circular cylinder wake stability (Henderson 1997).

4.1. *The Mode I regime* ($0 \leqslant Ar < 1.6$)

In this section, the non-axisymmetric wakes which evolve from the regular and Hopf transitions in the Mode I regime are computed and analysed.

4.1.1. *Wake structure after the regular non-axisymmetric transition*

The saturated non-axisymmetric wakes following the Mode I transition are depicted by streamwise vorticity isosurface plots in figure 3. For comparison, the same visualization for the flow past a sphere ($Ar = 0$) is also included. Flow is from the upper right corner to the lower left corner in each case. The ring/sphere is visible at the upper right of each frame. The light and dark isosurfaces represent negative and positive streamwise vorticity respectively, highlighting significant streamwise vorticity in the wake. It is apparent from these isosurface plots that a plane of symmetry exists in the wake through the centre of the ring. This symmetry has also been observed

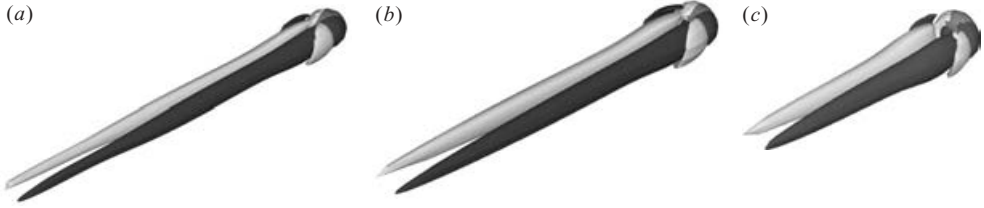(*a*)   (*b*)   (*c*)

FIGURE 3. Isosurface plots of streamwise vorticity showing the structure of the non-axisymmetric wakes which evolve in the flow past rings after the evolution of the regular transition in the Mode I regime. The flow past a sphere at $Re = 270$ is shown in (*a*), and the flows past a closed ring with $Ar = 0.6$ and an open ring with $Ar = 1.2$, are shown in (*b*) and (*c*), at $Re = 130$ and $Re = 85$, respectively. Light and dark grey isosurfaces represent negative and positive streamwise vorticity, respectively. The ring is located at the upper right corner, and flow is from the top right to the bottom left in each frame.

for the sphere (Tomboulides & Orszag 2000; Johnson & Patel 1999). Furthermore, this Mode I transition has $m = 1$ azimuthal symmetry, i.e. there is a single azimuthal wavelength spanning the azimuthal domain (2π). The similarity of figures 3(*b*) and 3(*c*) indicates that the flow fields are indeed both products of the growth and saturation of the previously predicted Mode I transition, and that the emergence of a small hole on the axis of the ring in this transition regime does not significantly modify the transition process. Note the wings of streamwise vorticity immediately behind the ring, and the pair of vorticity tails stretching far downstream. The latter correspond to the classic 'double-threaded wake' observed in the flow past a sphere (Tomboulides & Orszag 2000; Thompson *et al.* 2001*a*; Magarvey & Bishop 1961*a,b*) following the first non-axisymmetric transition.

4.1.2. *Application of the Landau model to the regular transition*

Due to the similarity between the non-axisymmetric wake structures of the regular Mode I wake throughout the Mode I regime, only one aspect ratio ($Ar = 0.6$) is used to study the nonlinear transition characteristics.

Figure 4 shows the nonlinear evolution behaviour of the regular Mode I transition. The negative slope near to the *y*-axis in figure 4(*b*) indicates that the transition occurs through a supercritical bifurcation. Thus it is expected that the transition will not be hysteretic. This is in agreement with the work by Ghidersa & Dušek (2000) and Thompson *et al.* (2001*a*), who identify similar behaviour for the regular non-axisymmetric transition in the flow past a sphere.

The critical Reynolds number for the regular Mode I transition in the flow past a ring with $Ar = 0.6$ was determined from the variation in growth rate (σ) with Reynolds number. The resulting critical Reynolds number matched the predicted transition Reynolds number from linear stability analysis (Sheard *et al.* 2003) to within 0.5%, in which case $Re_c = 114$ was ascertained. Figure 5 gives the variation in growth rate with Reynolds number for the flow past a ring with $Ar = 0.6$ from figure 4. Both the previous Floquet analysis and an independent quadratic fit to the current data provide a critical Reynolds number at this aspect ratio of $Re_c = 114$.

In figure 6(*a*), a plot of $|A|^2$ against $Re - Re_c$ is presented for the regular transition in the flow past ring with $Ar = 0.6$. The linear profile near to the transition ($Re - Re_c = 0$) supports the prediction that the transition is supercritical. Furthermore, the critical Reynolds number of the regular transition is confirmed to be $Re_c \approx 114$.
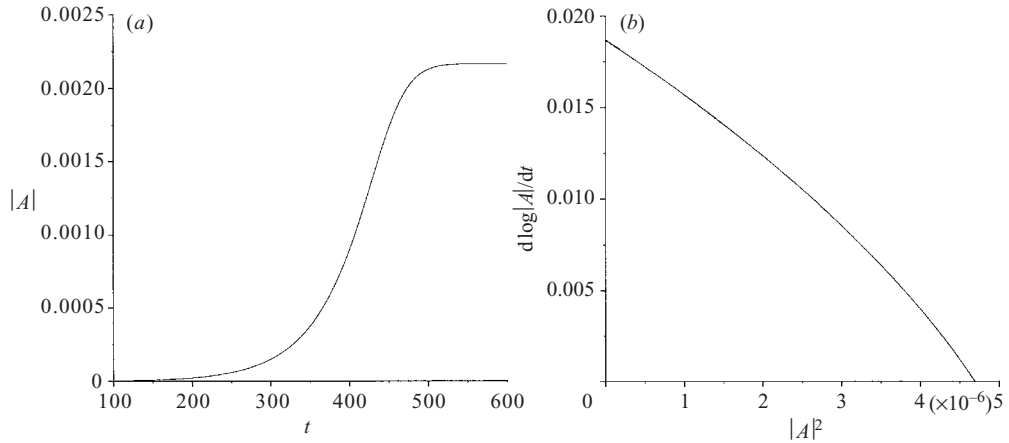
FIGURE 4. (*a*) The growth and saturation of the non-axisymmetric transient in the flow past a ring with $Ar = 0.6$ at $Re = 120$. (*b*) The derivative of the amplitude logarithm against the square of the amplitude. The *y*-axis intercept gives growth rate (σ) and the gradient close to the *y*-axis gives the saturation term, *l*. The negative slope and linear behaviour in the vicinity of the *y*-axis indicate that the transition is supercritical.
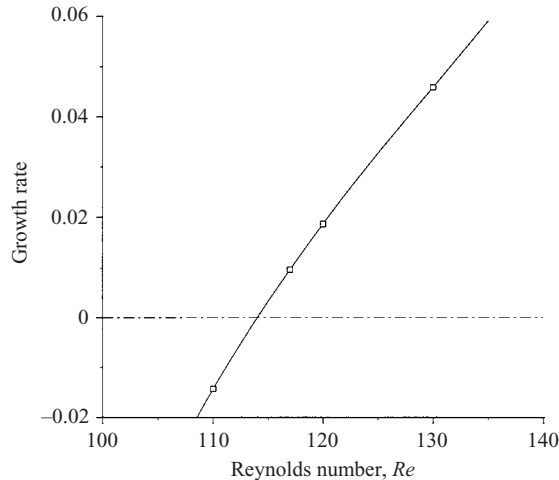

FIGURE 5. The growth rates from the Landau model computed in the vicinity of the regular transition in the Mode I regime in the flow past a ring with $Ar = 0.6$. Cubic interpolation gives $Re_c = 114$.

4.1.3. *Wake structure after the non-axisymmetric Hopf transition*

Over the aspect ratio range $0 \leqslant Ar < 1.6$, the regular Mode I transition is followed by a Hopf transition to unsteady flow at higher Reynolds numbers. For the flow past a sphere this transition occurs at $Re = 272$ (Thompson *et al.* 2001*a*; Johnson & Patel 1999), and the resulting wake is planar-symmetric, with $m = 1$ azimuthal symmetry. Numerical visualization of the vortical wake structure typically shows hairpin-shaped vortex loops shedding alternately from opposite sides of the axis, whereas experimental flow visualization can indicate hairpins aligned on one side of the axis only, depending on the location of the dye injection point.
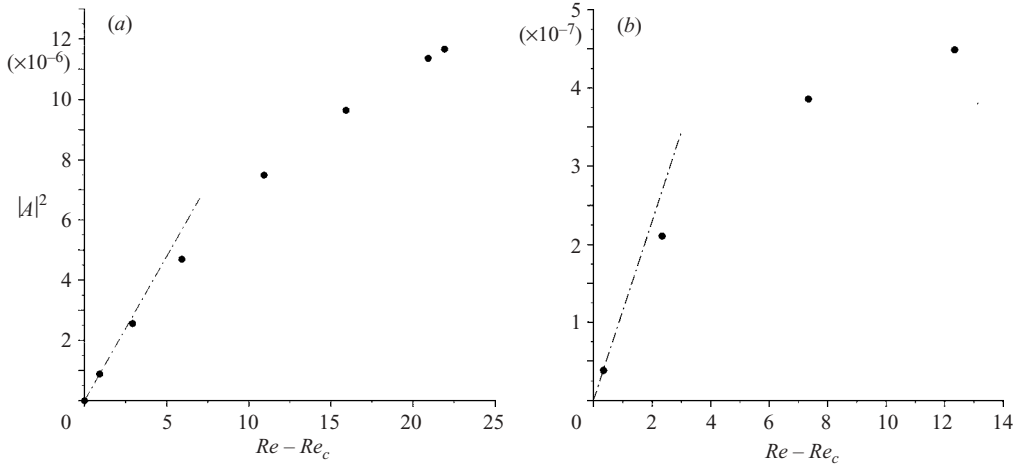
FIGURE 6. Plots which show a linear relationship between $|A|^2$ and $Re - Re_c$ in the vicinity of the transitions for both the (*a*) regular and (*b*) Hopf transitions in the flow past a ring with $Ar = 0.6$ in the Mode I regime. The solid circles represent the measured amplitudes, and the lines indicate the tangent to the data in the vicinity of $Re - Re_c = 0$.

Interestingly, the wakes computed at Reynolds numbers above the Hopf transition are remarkably similar in structure to the unsteady flow past a sphere. Figure 7(*a–c*) shows the wakes of a sphere, and rings with aspect $Ar = 0.6$ and $Ar = 1.2$, respectively.

Notice that the hairpin vortex structures, the vertical plane of symmetry, and the $m = 1$ azimuthal symmetry of the wakes are consistent throughout the Mode I regime.

4.1.4. *Application of the Landau model to the Hopf transition*

The nonlinear evolution of the Hopf transition in the Mode I regime is presented in figure 8. The negative slope and linear trend of the plot in figure 8(*b*) suggests that the Hopf transition occurs through a supercritical bifurcation, which again predicts a non-hysteretic transition. This is consistent with previous studies of the flow past a sphere, which predicted that the Hopf bifurcation following the regular non-axisymmetric transition is supercritical (Thompson *et al.* 2001*a*).

In figure 6(*b*), a plot of $|A|^2$ against $Re - Re_c$ is presented for the envelope of the Hopf transition as the wake saturates in the flow past a ring with $Ar = 0.6$. The trend of $|A|^2$ as $Re - Re_c \rightarrow 0$ supports the Landau model prediction that the transition occurs through a supercritical bifurcation. The critical Reynolds number for this transition is $Re_c \approx 137.7$.

The value of the Landau constant was calculated to be $c = -0.5 \pm 0.05$ in the vicinity of the secondary transition for the ring with $Ar = 0.6$. The Landau constant for the Hopf transition in the flow past a sphere has been shown to be $c = -0.55$ (Ghidersa & Dušek 2000; Thompson *et al.* 2001*a*), which is close to the value we find for the flow past a ring with $Ar = 0.6$.

4.1.5. *Bifurcations in the Mode I regime*

To verify the predictions pertaining to the hysteretic properties of the regular and Hopf transition modes in the Mode I regime, saturated amplitudes are computed at several Reynolds numbers close to the transition. Where the saturated wakes are
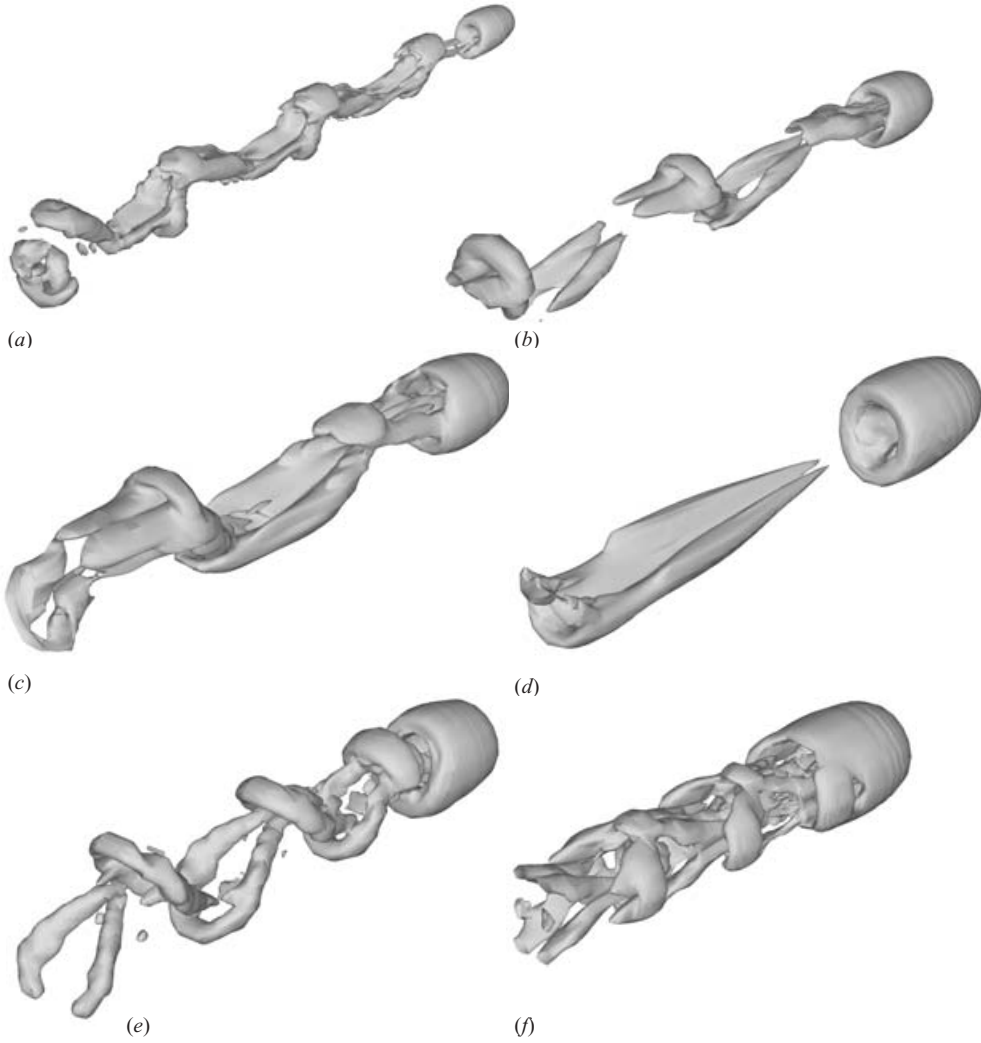
FIGURE 7. Isosurface plots of the unsteady wakes in the flow past rings with (*a*) $Ar = 0$, (*b*) $Ar = 0.6$, (*c*) $Ar = 1.2$, (*d*) $Ar = 1.6$, (*e*) $Ar = 2.0$ and (*f*) $Ar = 3.0$. (*a–c*) Computed at $Re = 300$, $Re = 160$ and $Re = 120$, respectively, and evolved from the Hopf transition in the Mode I regime. (*d*) Computed at $Re = 100$, and evolved from the Hopf transition in the Mode II regime. (*e–f*) Computed at $Re = 150$ and $Re = 138$, and evolved from the Hopf transition in the Mode III regime. The method of Jeong & Hussain (1995) was used to visualize the vortical structure of the wakes. Note the plane of symmetry through the centre of each ring, and the consistent vortical structure of the wakes. Flow is from the top right to the bottom left in each frame.

unsteady, maximum and minimum amplitudes are obtained to determine the envelope of oscillation.

Figure 9 presents the change in mode amplitude throughout a Reynolds number range encompassing the regular and Hopf transitions of the flow past a ring with $Ar = 0.6$. The figure illustrates that both the regular and Hopf transitions occur through supercritical bifurcations, as no hysteresis is found in the vicinity of either transition. This is consistent with the predictions from the Landau modelling in previous sections, which predict $|A|^2 \propto (Re - Re_c)$.
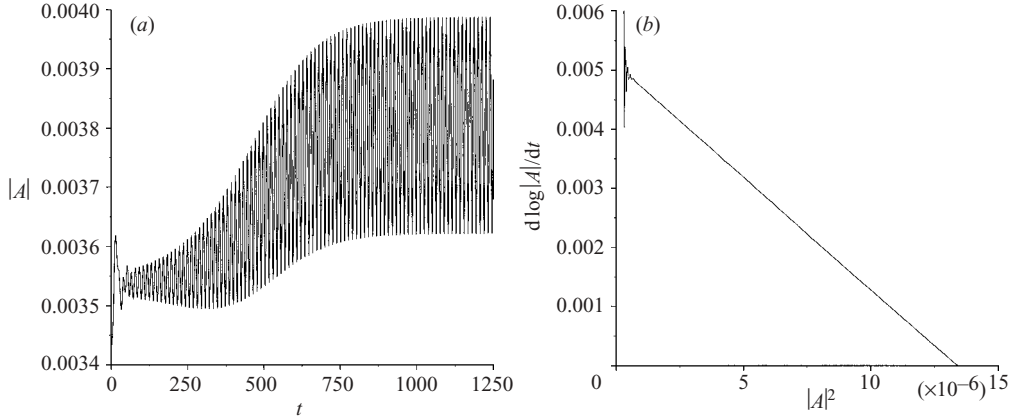
FIGURE 8. (*a*) The growth and saturation of the envelope of the non-axisymmetric transient in the flow past a ring with $Ar = 0.6$ at $Re = 139$. (*b*) The derivative of the amplitude logarithm against the square of the amplitude, which shows supercritical behaviour.
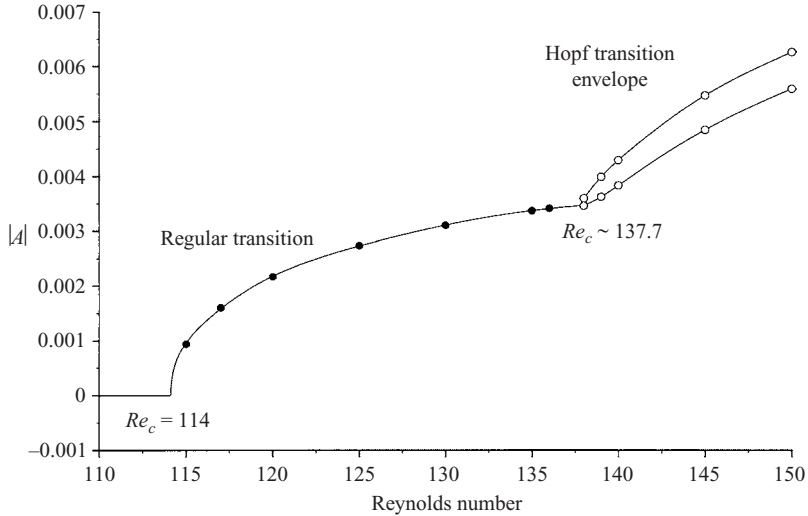

FIGURE 9. Non-axisymmetric regular and Hopf mode bifurcations of the flow past a ring with $Ar = 0.6$. Solid circles represent the computed mode amplitudes for the regular transition, and open circles show the maximum and minimum computed mode amplitudes of the envelope of oscillation of the Hopf transition. Lines show the likely transition branches.

4.2. *The Mode II regime* $(1.6 \leqslant Ar \leqslant 1.7)$

In this section, the non-axisymmetric wake which evolves from the Hopf transition in the Mode II regime is computed and analysed.

4.2.1. *Wake structure after the non-axisymmetric Hopf transition*

The saturated wake structure following the Mode II transition is shown in figure 10, again visualized using streamwise vorticity isosurfaces. The near wake in this case is not dissimilar to the near-wake region for the Mode I transition directly behind the ring, with wings of streamwise vorticity of opposing sign wrapped around longer tails of streamwise vorticity extending downstream. However, rather than forming
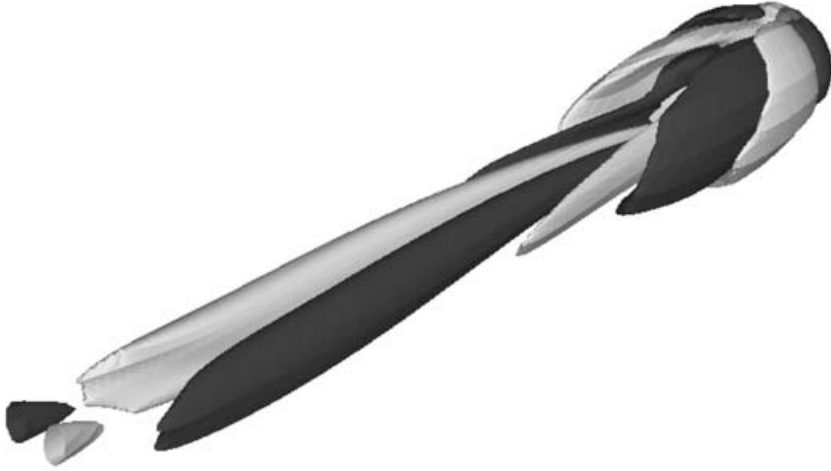
FIGURE 10. An instantaneous streamwise vorticity isosurface plot of the wake behind a ring with $Ar = 1.6$ at $Re = 100$ after the saturation of the Hopf transition in the Mode II regime. Isosurface contours and flow direction are as in figure 3.

the stationary double-threaded wake observed in the Mode I regime, the wake in the Mode II regime sheds long slanted pairs of vortices of alternating sign downstream. The Mode II transition is a Hopf transition from a steady axisymmetric flow to a non-axisymmetric unsteady flow. This is in close agreement with the predictions of the stability analysis of Sheard *et al.* (2001, 2003) for this transition, which indicated that the most amplified Floquet mode was periodic, corresponding to a Hopf bifurcation to a periodic non-axisymmetric wake. Note that the planar symmetry and the $m = 1$ azimuthal symmetry, observed for the Mode I regime, are retained for the Mode II transition.

The same flow field may also be compared with the Hopf transition wakes of rings in the Mode I and Mode III regimes. Figure 7(d) shows the wake computed after the Mode II Hopf transition in the flow past a ring with $Ar = 1.6$ at $Re = 100$. The wake differed from the unsteady wakes computed in the Mode I and Mode III regimes, as the saturated state was not periodic and the average Strouhal frequency was approximately 30% of the Strouhal frequency associated with the Hopf transitions in the Mode I and Mode III regimes. The isosurface plot of the Mode II wake has been obtained from the same velocity field as the streamwise vorticity plot from figure 10. Structurally the Mode II wake is different to the other wakes resulting from Hopf transitions. Instead of the hairpin wake, with vortices being shed either side of the axis, long bands of vorticity are cast into the wake on one side of the axis.

4.2.2. *Application of the Landau model to the Hopf transition*

To model the nonlinear behaviour of the Mode II transition, the envelope of the oscillation of the L_2 norm was calculated. Figure 11 shows the nonlinear evolution of the non-axisymmetric Hopf transition in the flow past a ring with $Ar = 1.6$ at $Re = 98$.

The negative slope observed near to the axis in figure 11(b) indicates that the Mode II transition occurs through a supercritical bifurcation. The evolution of the mode in figure 11(a) shows that despite the large period of oscillation, sufficient data points have been obtained to predict the transition bifurcation type. The Landau constant measured within the vicinity of the Mode II transition was found to be
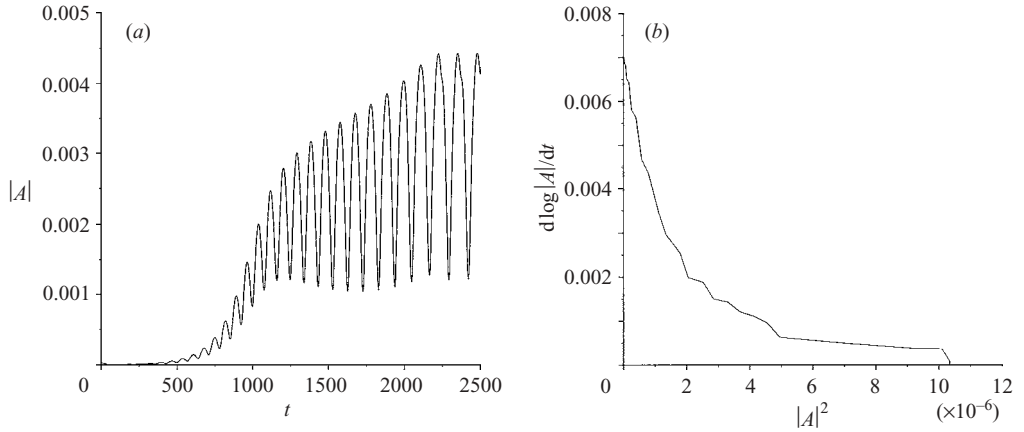
FIGURE 11. (*a*) The growth and saturation of the envelope of the non-axisymmetric transient in the flow past a ring with $Ar = 1.6$ at $Re = 98$. (*b*) The derivative of the amplitude logarithm against the square of the amplitude, which shows supercritical behaviour.
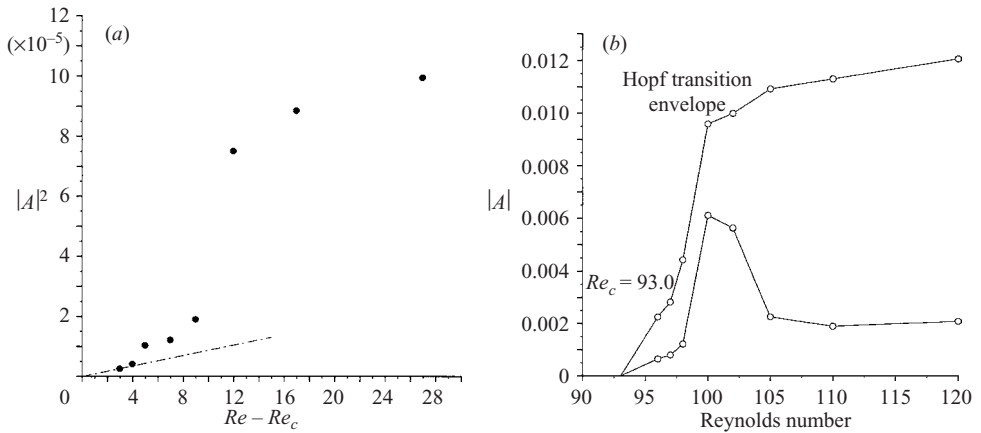

FIGURE 12. Plots of the evolution of the Mode II transition in the flow past a ring with $Ar = 1.6$. (*a*) The square of the envelope of the unsteady azimuthal amplitude against $Re - Re_c$. The dotted line shows a possible linear fit to the data in the vicinity of $Re - Re_c = 0$, and solid circles show the computed data points. (*b*) The azimuthal mode amplitude variation with Reynolds number. Open circles represent the maximum and minimum computed mode amplitudes at a given Reynolds number, and lines show the maximum and minimum limits to the oscillation envelope of the mode amplitude.

$c = -0.60$. This value was obtained at $Re - Re_c = 3.5$, for a ring with $Ar = 1.6$, and was measured from the velocity signal at a point in the wake approximately $4d$ downstream of the ring cross-section.

4.2.3. *Bifurcations in the Mode II regime*

The spontaneous inception of a non-axisymmetric and unsteady wake that occurs following the Mode II transition is highlighted by the plots in figure 12. In figure 12(*a*), a plot of the variation of the envelope of the amplitude with $Re - Re_c$ is presented. The plot verifies that the Landau model correctly predicts that the Mode II transition occurs through a supercritical bifurcation. In figure 12(*b*), a plot of the variation in
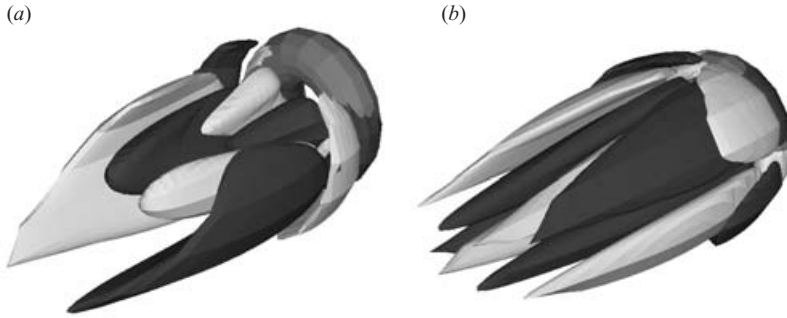
(*a*)   (*b*)

FIGURE 13. Streamwise vorticity isosurface plots of the wakes behind (*a*) a ring with $Ar = 2$ at $Re = 100$ and (*b*) a ring with $Ar = 3$ at $Re = 115$, after the evolution of the regular transition in the Mode III regime. Note the change in symmetry between the two aspect ratios. Isosurface contours are as in figure 3.

$|A|$ with Reynolds number is presented. The supercritical nature of the transition is again highlighted, as both the maximum and minimum amplitude profiles first become non-zero ($|A| \geqslant 0$) continuously at $Re_c \approx 93$. The absence of steady non-axisymmetric wakes for $Re > Re_c$ supports the stability analysis of Sheard *et al.* (2003), that predicts the Mode II instability is a complex-conjugate Floquet mode.

4.3. *The Mode III regime* ($1.7 \lesssim Ar \lesssim 3.9$)

In this section, the non-axisymmetric wakes which evolve from the regular and Hopf transitions in the Mode III regime are computed and analysed.

4.3.1. *Wake structure after the regular non-axisymmetric transition*

The flow past a ring following the Mode III transition is shown in figure 13. This mode evolves from a regular (steady–steady) transition, as does Mode I; however, structurally it is vastly different to Mode I. Instead of long tails of streamwise vorticity extending far downstream along the axis, bands of vorticity are localized in the wake directly downstream of the ring body. As with the Mode I transition, the wake structures indicate that the transition involves a loss of stability of the recirculation region behind the ring body; however, in the case of the Mode III transition, the recirculation bubble is located directly behind the ring body, rather than on the axis.

The Mode III transition is observed for rings with aspect ratios $1.8 \lesssim Ar \lesssim 3.9$. At larger aspect ratios ($Ar \gtrsim 3.9$), the non-axisymmetric transition is preceded by a Hopf bifurcation to a periodic axisymmetric wake, similar to the von Kármán vortex street for a circular cylinder wake. The $m = 1$ azimuthal symmetry of the instability associated with the Mode III transition is not maintained throughout its aspect ratio range $1.8 \leqslant Ar < 4$. Stability analysis of the flow past a ring with $Ar = 3$ (Sheard *et al.* 2003) predicted an azimuthal symmetry of $m = 2$, the remnants of which can be observed in figure 13(*b*). The $m = 2$ azimuthal symmetry is associated with perpendicular planes of symmetry intersecting the axis. The azimuthal symmetry of the wake in figure 13(*a*) corresponds to an instability with $m = 1$ symmetry.

To further illustrate the changes in azimuthal symmetry and flow structure for the Mode III transition with increasing aspect ratio, the isosurfaces plots from figure 13 are shown in figure 14 with the wake viewed from directly behind the ring. Note in figure 14 the structural similarity between the Mode III wake for the two rings. If one were to imagine making a cut through the ring in figure 14(*a*) at the top of the frame, and azimuthally bending the ring and the wake into a semicircle, the shape

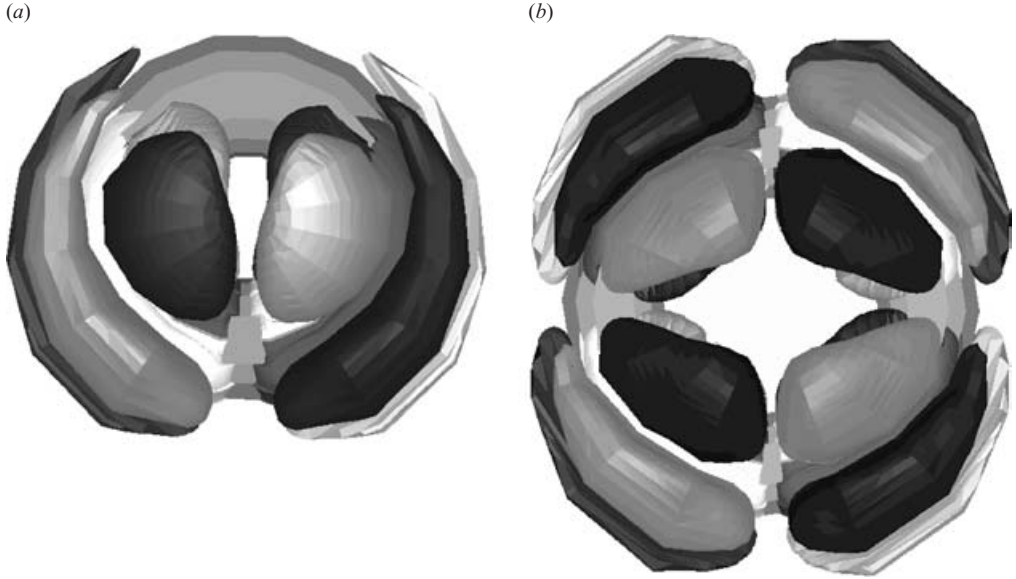(*a*)   (*b*)

FIGURE 14. Isosurface plots of streamwise vorticity which show the $m = 1$ and $m = 2$ azimuthal symmetries of the wakes after the evolution of the regular transitions in the Mode III regime for the flow past rings with (*a*) $Ar = 2$ and (*b*) $Ar = 3$, respectively. The rings are viewed from directly downstream, and the isosurface shading is as in figure 3.

of the non-axisymmetric structures would almost exactly match those present over half the ring in figure 14(*b*). This observation suggests that it is correct to classify both of these wakes as Mode III transition wakes. Furthermore, it suggests that this mode scales with the lengthscale for the cross-section of the ring (d), rather than the entire ring ($D + d$). If the steady non-axisymmetric transition were not impeded by the axisymmetric Hopf bifurcation in the flow past rings with $Ar \gtrsim 3.9$, then one would expect to find a Mode III transition in the flow past rings for all aspect ratios $Ar \gtrsim 1.8$, with an azimuthal wavelength based on the ring cross-section diameter, d.

4.3.2. *Application of the Landau model to the regular transition*

The evolution of the amplitude of the regular Mode III transition as it saturates for a ring with $Ar = 2$ at $Re = 93$ is shown in figure 15. In figure 15(*b*), the distinct nonlinearity and positive gradient at the y-intercept suggest that the Mode III transition occurs through a subcritical bifurcation. This indicates that higher-order terms are required for the Landau model to completely describe the saturation of this transition.

To verify that the regular Mode III transition is subcritical, a plot of $|A|^2$ against $Re - Re_c$ is provided in figure 16(*a*). It is clear that the mode amplitude does not approach zero as $Re - Re_c \to 0$. The computation of a steady non-axisymmetric wake below the transition Reynolds number verifies that the onset of the regular transition is hysteretic. This supports the prediction of the Landau model that the transition evolves through a subcritical bifurcation.

4.3.3. *Wake structure after the non-axisymmetric Hopf transition*

The wakes observed following the Hopf transition in the Mode III regime show a change in symmetry with increasing aspect ratio, maintaining the azimuthal
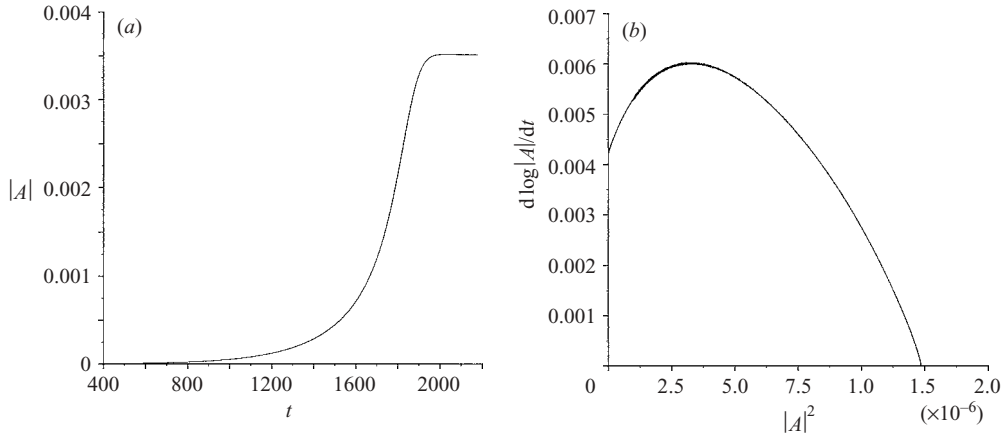
FIGURE 15. (*a*) The growth and saturation of the non-axisymmetric transient in the flow past a ring with $Ar = 2$ at $Re = 93$. (*b*) The derivative of the amplitude logarithm against the square of the amplitude. The positive gradient and nonlinear behaviour near the *y*-axis indicates that the transition is subcritical.
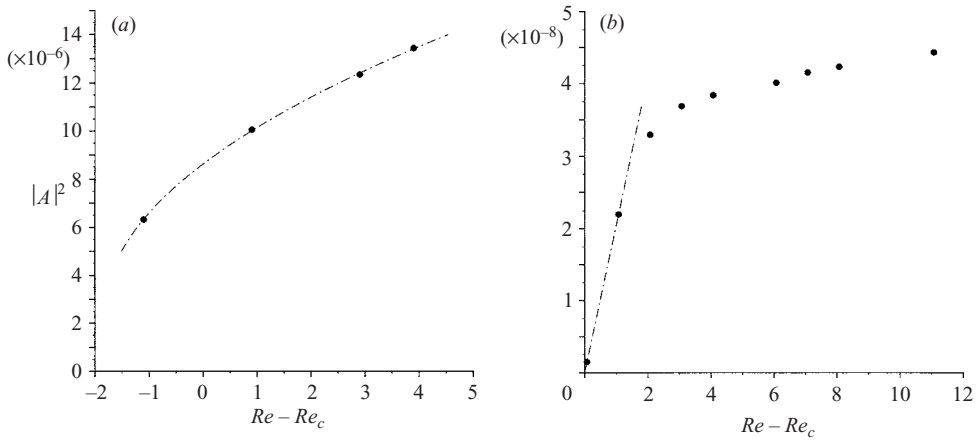

FIGURE 16. $|A|^2$ against $Re - Re_c$ for the (*a*) regular and (*b*) Hopf transitions in the flow past a ring with $Ar = 2$. Solid circles represent the computed amplitudes, and the dotted lines provide a linear fit to the data. The subcritical nature of the regular transition is evident in (*a*), as is the continuous supercritical Hopf bifurcation behaviour in (*b*).

symmetry properties of the regular Mode III transition that were highlighted earlier. Figure 7(*e*, *f*) shows the wakes which result from instabilities with azimuthal symmetries $m = 1$ and $m = 2$, in the flows past rings with $Ar = 2$ and $Ar = 3$, respectively, consistent with the regular transitions of the same rings. The hairpin structure and symmetry of figure 7(*e*) is well-defined, and is analogous to the post-Hopf transition wakes computed for the Mode I regime. Figure 7(*f*) shows a symmetry consistent with an $m = 2$ instability, with both horizontal and vertical planes of symmetry. Interestingly, miniature hairpin structures may also be observed near to the core of the wake in figure 7(*f*). These structures form on the inner surface of the ring, and appear to increase in prominence with increasing size of the ring orifice.
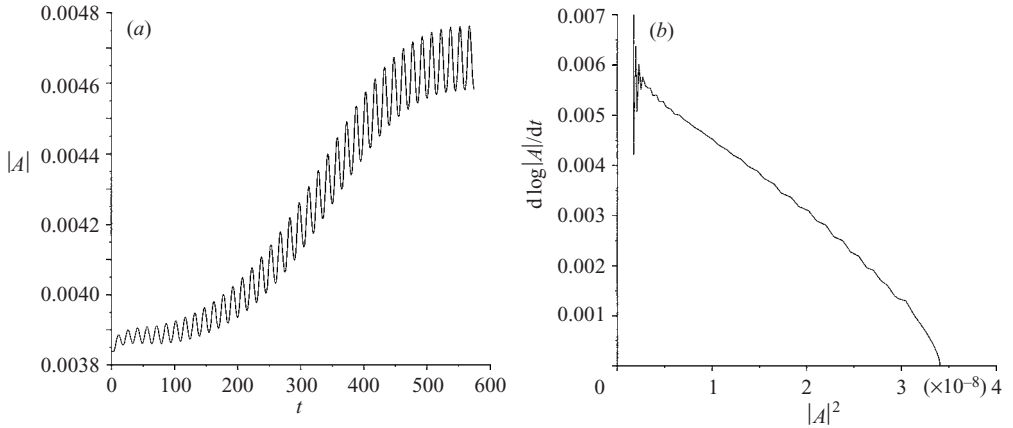
FIGURE 17. (*a*) The growth and saturation of the envelope of the non-axisymmetric Hopf transition in the flow past a ring with $Ar = 2$ at $Re = 96$. (*b*) The derivative of the amplitude logarithm against the square of the amplitude, which indicates supercritical behaviour. A linear growth rate of approximately $\sigma \approx 0.006$ and a negative slope is observed in the vicinity of the *y*-axis.

4.3.4. *Application of the Landau model to the Hopf transition*

The previous subsections have shown that both the Hopf transition subsequent to the Mode I transition, and the Mode II Hopf transition, are supercritical. The evolution of the Hopf transition that occurs after the regular Mode III transition for a ring with $Ar = 2$ is presented in figure 17(*a*). The real coefficients of the Landau model are determined from figure 17(*b*), which shows behaviour consistent with a supercritical bifurcation. The wiggles present near to the *y*-axis in figure 17(*b*) are an artefact of the initial conditions for the computation, where a steady-state non-axisymmetric flow field computed just below the unsteady transition Reynolds number ($Re = 93 < Re_c \approx 94$) was employed.

In figure 16(*b*) a plot showing the variation in $|A|^2$ with $Re - Re_c$ is presented. This plot highlights the linear evolution of the square of the mode amplitude envelope with $Re - Re_c$. This continuous mode evolution is consistent with a supercritical bifurcation, supporting the Landau model prediction pertaining to this Hopf transition.

The Landau constant was calculated for the Hopf transition in the Mode III regime at aspect ratios of $Ar = 2$ and $Ar = 3$. For the ring with $Ar = 2$ the Landau constant is $c = -0.92$, and for $Ar = 3$ the Landau constant takes the value $c = -4.1$.

4.3.5. *Bifurcations in the Mode III regime*

The bifurcations to non-axisymmetry in the Mode III regime are possibly the most interesting of the bifurcations of any of the three aspect ratio regimes treated thus far. The plot in figure 18 shows the variation in the non-axisymmetric mode amplitude with Reynolds number for the flow past a ring with $Ar = 2$. Both stability analysis and the present computations found that a regular non-axisymmetric mode evolved in the wake for $Re > Re_c$, where $Re_c \approx 90.1$. A region of hysteresis is observed for a Reynolds number range below Re_c, supporting the Landau model prediction that the regular Mode III transition occurs through a subcritical bifurcation.

The steady non-axisymmetric wake becomes temporally unstable for Reynolds numbers beyond $Re \approx 94$. On reducing the Reynolds number, this Hopf transition
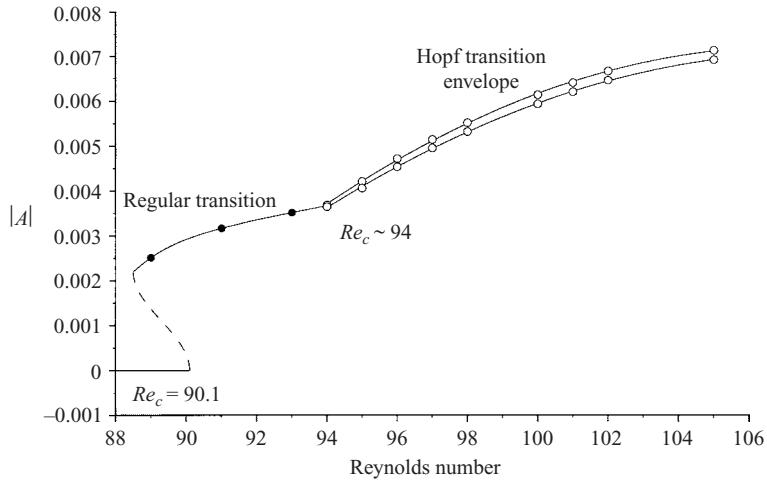
FIGURE 18. Mode amplitude variation against Reynolds number for the non-axisymmetric transitions in the flow past a ring with $Ar = 2$. The dashed line highlights the hysteretic onset of the regular transition, and solid lines show the regular and Hopf transition branches. Computed data points for the regular transition branch and the Hopf transition envelope are represented by solid and open circles, respectively.

decayed to a steady state for all Reynolds numbers below the transition Reynolds number, confirming the prediction that the Hopf transition is supercritical.

5. Results II: variation of Landau model constants with aspect ratio

The previous section presented the calculated Landau constant (c) values that were obtained for the first-occurring Hopf transition for rings with aspect ratios in the range $Ar \lesssim 3.9$. This section presents results of calculations of c for the axisymmetric Hopf transition of rings with aspect ratios $Ar \gtrsim 3.9$. Specifically, Landau constants are calculated for the Hopf transitions for aspect ratios $Ar = 4, 5, 10, 20$ and 40.

In addition, the Landau diffusivity constant is evaluated over the entire aspect ratio range for the present study, to examine the behaviour of this parameter for the limiting cases previously reported in the literature. A Landau diffusivity constant of approximately 5 has been calculated for the Hopf transition in the flow past a circular cylinder by Provansal *et al.* (1987). From data presented by Thompson *et al.* (2001*a*) for the Hopf transition in the flow past a sphere, a value of approximately 1.86 is obtained.

A complete profile of the Landau constant variation with aspect ratio is presented in figure 19(*a*). It is important to note the consistency between the Landau constants measured at both $Ar = 0.6$ and $Ar \geqslant 5$, and accepted values for the Landau constant of a sphere and straight circular cylinder ($c = -0.55$ and $-3.0 < c < -2.6$, respectively).

The most interesting feature of this variation is the significantly greater magnitude of the computed value of c at $Ar \approx 4$, near the crossover point in aspect ratio parameter space for the Hopf transition and non-axisymmetric transition. The larger amplitude was due to a combination of a larger frequency shift through saturation of the wake and a smaller growth rate of the instability than was measured for most of the aspect ratio range.

The aspect ratio $Ar \approx 4$ delineates two regimes. For aspect ratios $Ar \gtrsim 4$, the Hopf transition occurs prior to a non-axisymmetric transition. The small variation in
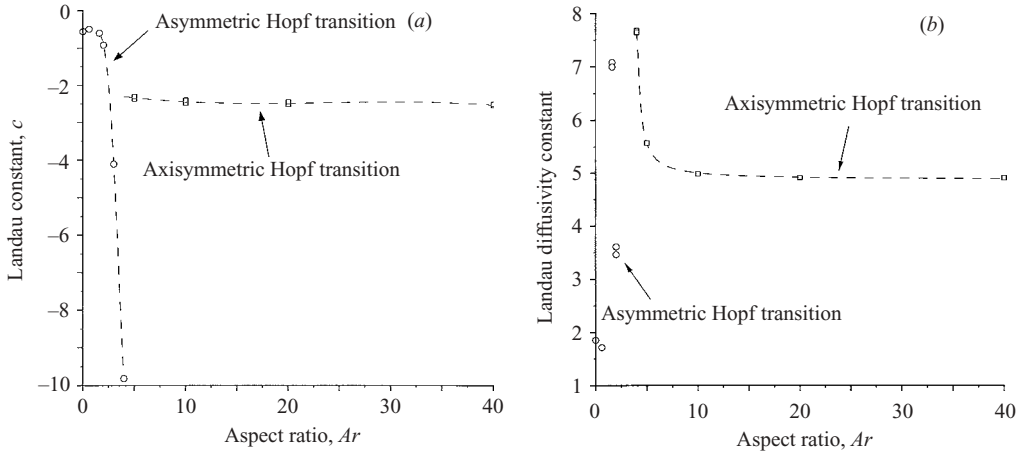
FIGURE 19. (*a*) The Landau constant (*c*) against *Ar*. (*b*) The Landau diffusivity constant against *Ar*. The Landau constants are calculated within the vicinity of the primary Hopf transition of the wake at each aspect ratio.

measured constants throughout this aspect ratio range is probably due to the similarity in the von Kármán shedding wakes obtained. As shown earlier, for $Ar \lesssim 4$, the Hopf transitions bifurcate from steady non-axisymmetric wakes (except the Mode II transition). The structure of the post-Hopf transition wakes observed for aspect ratios $Ar \lesssim 4$ is very different to the range $Ar \gtrsim 4$, and it is unsurprising, therefore, that the variation in the constants throughout these two regimes is so different.

Figure 19(*a*) shows that for smaller aspect ratios ($0 \leqslant Ar \lesssim 4$), the Landau constant varies between $c = -0.554$ and $c = -9.8$. For larger aspect ratios ($Ar \gtrsim 4$), the Landau constant asymptotes towards a constant, decreasing from $c = -2.37$ at $Ar = 5$ to $c = -2.55$ at $Ar = 40$.

Figure 19(*b*) shows the variation in the Landau diffusivity constant with aspect ratio. Notice that the values of the constant over the axisymmetric Hopf transition range ($Ar \gtrsim 4$) rapidly asymptote to approximately 5 with increasing aspect ratio, consistent with the value obtained by Provansal *et al.* (1987) for the flow past a circular cylinder. There is little consistency in the measured data points for the non-axisymmetric Hopf transition ($Ar \lesssim 4$), with values obtained in the vicinity of 1.8, 7 and 3.5, for the Mode I, Mode II and Mode III transitions, respectively. This highlights the different wakes that the Hopf transition bifurcates from in each of the transition regimes. Notice that a value of 1.72 is obtained for an aspect ratio of $Ar = 0.6$. This is close to the value of 1.86 obtained for the Hopf transition in the flow past a sphere from the data presented in Thompson *et al.* (2001*a*).

6. Results III: large aspect ratios ($Ar \gtrsim 3.9$)

The occurrence of linear instabilities in the vortex street in flow past rings has been predicted by stability analysis (Sheard *et al.* 2003). Experimental Strouhal number profiles have also indicated the presence of transitions in the vicinity of the critical Reynolds number for the Mode A and Mode B transitions for the circular cylinder (Leweke & Provansal 1995). The results of non-axisymmetric computations are presented here to verify the predictions of the earlier stability analysis, and to classify the structural and hysteretic properties of the modes.

Ar	First mode	Second mode	Third mode
5	Mode C ($Re_C \approx 163.3$)	†Mode A ($Re_A \approx 194.0$)	Mode B ($Re_B \approx 301.4$)
10	Mode A ($Re_A \approx 194.3$)	Mode C ($Re_C \approx 222.1$)	Mode B ($Re_B \approx 270.0$)
20	Mode A ($Re_A \approx 189.2$)	Mode B ($Re_B \approx 261.2$)	†Mode C ($Re_C \approx 310.9$)

TABLE 1. The order in which the non-axisymmetric instabilities are predicted to occur in the flow past the rings selected for the present study. Predicted critical Reynolds numbers (Sheard *et al.* 2003) from Floquet analysis are also provided. †Modes not computed in the present study due to an inability to isolate the pure mode.

Three representative aspect ratios have been selected to study the non-axisymmetric instabilities in the flow past rings. These are $Ar = 5$, 10 and 20, and were selected based on the interesting wake stability predictions of Sheard *et al.* (2003), where it was noted that the order of occurrence of the non-axisymmetric instabilities varied with aspect ratio. This phenomenon results due to the wide variation in the critical Reynolds number for the onset of the Mode C instability, which varies from $Re_c \approx 163.3$ at $Ar = 5$ to $Re_c \approx 310.9$ at $Ar = 20$. Table 1 gives the predicted instabilities for the flow past the three rings investigated in this section.

Despite the ability to isolate non-axisymmetric instability modes by limiting the computational domain, only the first-occurring mode is physically significant, as in practice the flow past a ring has no such restriction. For this reason, the reported nonlinear transition properties in the subsections to follow focus on the first-occurring non-axisymmetric instability in the wake. For completeness, and due to the interest in the subharmonic Mode C instability, the predictions of the nonlinear transition properties of the subsequent instabilities modes from the application of the Landau model are briefly reported. Consistent with the application of the Landau model to the flow past rings with $Ar \lesssim 3.9$, an L_2 norm was computed to evaluate the Landau model coefficients for the evolution of non-axisymmetric flow in the wakes of rings with $Ar = 5$, 10 and 20.

6.1. *Wake instability mode path C–A–B: $Ar = 5$*

In this subsection iso-surface plots and the results of the application of the Landau model to the evolution of the non-axisymmetric modes in the flow past a ring with $Ar = 5$ are presented.

6.1.1. *Wake structure after the Mode C transition*

The first non-axisymmetric instability to occur in the flow past a ring with $Ar = 5$ is Mode C. An isosurface plot showing the structure of the wake which evolves from the Mode C instability is presented in figure 20(a). The Mode C instability is interesting as it is not found in the flow past a circular cylinder (Barkley & Henderson 1996; Williamson 1996), and it is predicted to be subharmonic (i.e. the instability occurs through $\mu = -1$, Sheard *et al.* 2003).

The plot of the wake structure in figure 20(a) highlights some interesting features of the saturated non-axisymmetic wake. Notice first that pairs of broad bands of opposite-sign streamwise vorticity are located above each vortex roller. Significantly, the sign of these vorticity bands alternates from one shedding cycle to the next. The vortex rollers are deformed into a wavy shape by the development of the streamwise vortity; however, in every shedding cycle the axial direction of deformation alternates with the sign of the vortex structures. The high curvature of a ring with $Ar = 5$ (relative to larger aspect ratios) alters the shape of the streamwise vortical structures
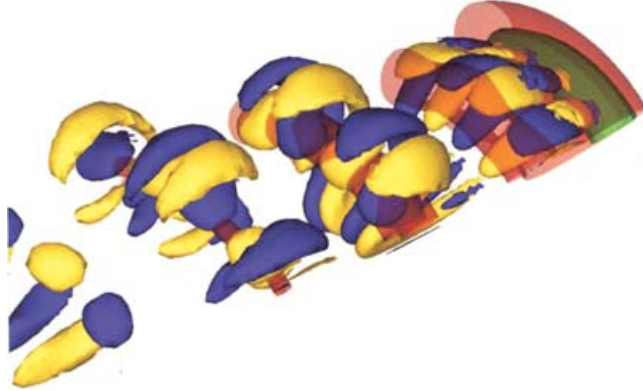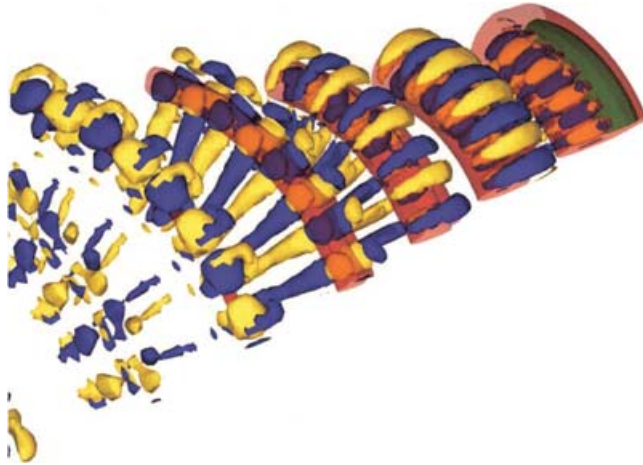
(*a*) Mode C, $\lambda_d \approx 2d$, $Re = 170$.

(*b*) Mode B, $\lambda_d \approx 1d$, $Re = 310$.

FIGURE 20. Isosurface plots showing the vortex structure of the non-axisymmetric flow past a ring with $Ar = 5$. Blue and yellow isosurfaces represent positive and negative streamwise vorticity, respectively, and red isosurfaces represent a pressure of -0.1, which shows the location of rollers in the vortex street. The ring is coloured green and is located at the upper right corner of each frame, and the flow direction is towards the lower left corner.

which form on the underside of the wake; however, an identical sign alternation takes place, and the sign of a streamwise vortex located on the underside of the wake is the same as the streamwise vortex located above the wake centreline from the preceding half-period. The wavelength of the saturated wake structures which evolve from the Mode C instability is approximately $1.7d$.

6.1.2. *Application of the Landau model to the Mode C transition*

In figure 21(*a*), the evolution of the amplitude of Mode C instability in the flow past a ring with $Ar = 5$ at $Re = 170$ is shown. Figure 21(*b*) is used to determine the cubic coefficients of the Landau model. The negative gradient at the y-axis suggests that the Mode C transition occurs here through a supercritical bifurcation. However, the nonlinear variation in the growth rate with $|A|^2$ suggests that at least fifth-order terms are required for the Landau model to describe the evolution of the Mode C instability in this flow.
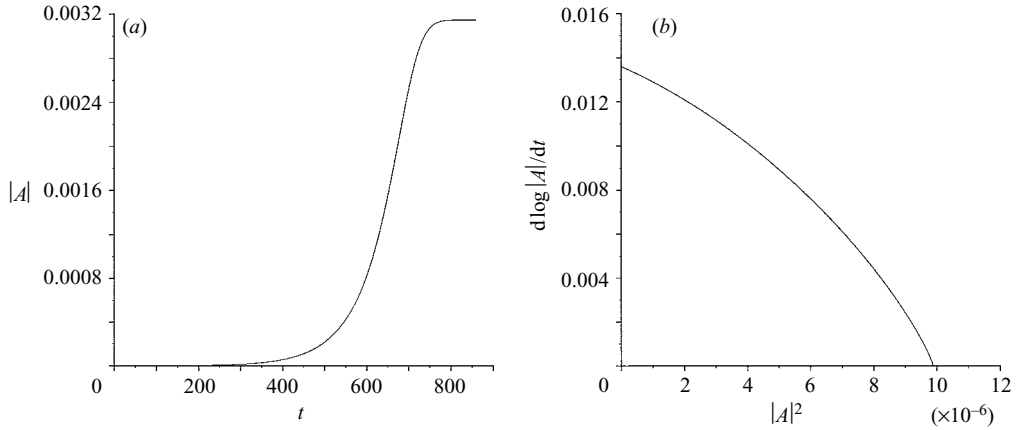
FIGURE 21. (*a*) The growth and saturation of the envelope of the non-axisymmetric transient corresponding to the Mode C instability of a ring with aspect ratio $Ar = 5$ at $Re = 170$. (*b*) The derivative of the amplitude logarithm against the square of the amplitude, showing supercritical behaviour.
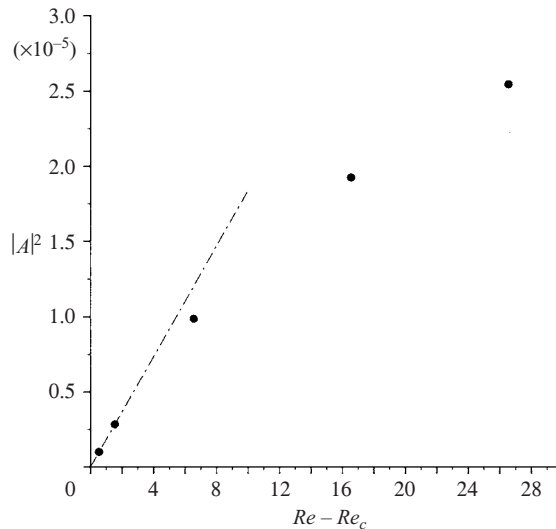

FIGURE 22. $|A|^2$ against $Re - Re_c$ for the Mode C instability in the flow past a ring with $Ar = 5$. $Re_c \approx 163.3$, and non-hysteretic behaviour is indicated.

An L_2 norm of the saturated non-axisymmetric wake was computed at several Reynolds numbers in the vicinity of the Mode C transition in the flow past a ring with $Ar = 5$. In figure 22, a plot of $|A|^2$ against $Re - Re_c$ is presented, which shows that the amplitude of the instability approaches zero as $Re - Re_c \to 0$, which verifies that no hysteresis is found at the onset of the transition, and that the transition occurs through a supercritical bifurcation.

6.1.3. *The secondary instability: wake structure and nonlinear transition properties*

The structure of the wake which was computed to capture the pure Mode B instability is shown in figure 20(*b*). Two features of the wake which are similar to

the Mode B wake observed in the flow past a circular cylinder (Thompson *et al.* 1996; Henderson 1997) are the azimuthal wavelength (approximately 0.8*d*) and the spatio-temporal symmetry of the non-axisymmetric wake structures.

An L_2 norm of the non-axisymmetry in the flow was monitored as the evolution of the Mode B instability was computed. In analysis, the Mode B transition was found to occur through a supercritical bifurcation. This predicted transition behaviour was confirmed by computations at several Reynolds numbers in the vicinity of Re_c.

6.2. *Wake instability mode path A–C–B: Ar = 10*

In this subsection iso-surface plots and the results of the application of the Landau model to the evolution of the non-axisymmetric modes in the flow past a ring with $Ar = 10$ are presented.

6.2.1. *Wake structure after the Mode A transition*

In figure 23(*a*), an isosurface plot is presented which shows the computed structure of the wake in which the Mode A evolved. Features in common with the Mode A wake observed in the flow past a circular cylinder (Thompson *et al.* 1996; Barkley & Henderson 1996) which are shown in the plot are the azimuthal wavelength of the instability (approximately 4*d*), the streamwise vorticity distribution, and the spatio-temporal symmetry.

The wake consists of spanwise vortex rollers that are deformed by the evolution of the non-axisymmetric Mode A instability. Every half-period, a pair of streamwise vortices entrains into the braid region on one side of the wake centreline from the vortex roller in which they evolved. These vortices deform the rollers of the vortex street. This process is repeated on alternating sides of the wake every half-period, and is described in detail in Williamson (1996) for the flow past a circular cylinder. The sign of the streamwise vortices remains constant from one period to the next, and they are opposite in sign to the pair of fingers which are located on the opposite side of the wake. This vorticity distribution means that the spatio-temporal symmetry of the velocity field is qualitatively similar to the spatio-temporal symmetry of the Mode A instability in the flow past a circular cylinder (Barkley & Henderson 1996), where a half-period shift in time and a reflection about the wake centreline yields an identical wake.

#### 6.2.2. *Application of the Landau model to the Mode A transition*

In figure 24(*a*), the evolution of the amplitude of Mode A instability in the flow past a ring with $Ar = 10$ at $Re = 200$ is shown. The plot in figure 24(*b*) was used to determine the cubic coefficients of the Landau model. The positive gradient in the vicinity of the *y*-axis and the approximately parabolic profile of the plot suggests that the Mode A transition occurs through a subcritical bifurcation.

In order to verify the subcritical transition behaviour predicted by the application of the Landau model, a plot of $|A|^2$ against $Re - Re_c$ is provided in figure 25. Saturated mode amplitudes were computed at several Reynolds numbers in the vicinity of the transition, and it is shown that the L_2 norm associated with the saturated Mode A wake did not approach zero as $Re - Re_c$ approached zero. This behaviour confirms that the a region of hysteresis is found at the onset of the transition, which is in agreement with the observed behaviour at the onset of the Mode A instability in the flow past a circular cylinder (Henderson 1997).

(*a*) Mode A, $\lambda_d \approx 4d$, $Re = 200$.
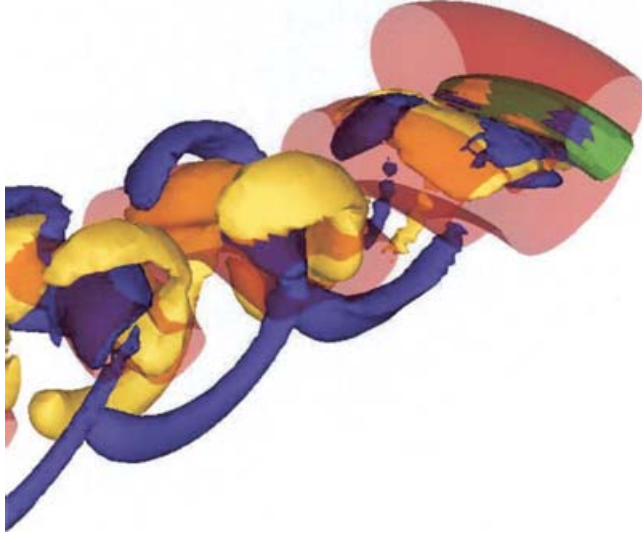
(*b*) Mode C, $\lambda_d \approx 2d$, $Re = 235$.
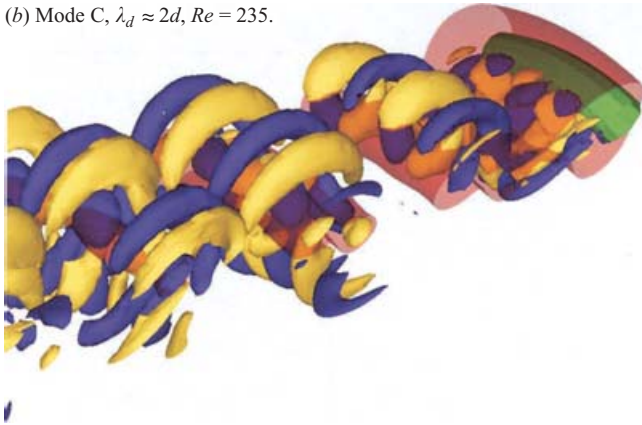
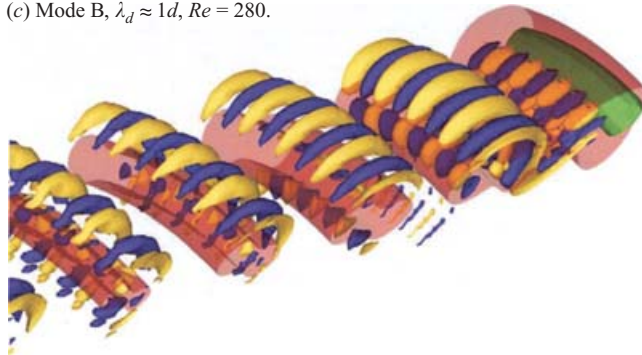(*c*) Mode B, $\lambda_d \approx 1d$, $Re = 280$.

FIGURE 23. Isosurface plots showing the vortex structure of the non-axisymmetric flow past a ring with $Ar = 10$. Isosurface colours are as in figure 20.
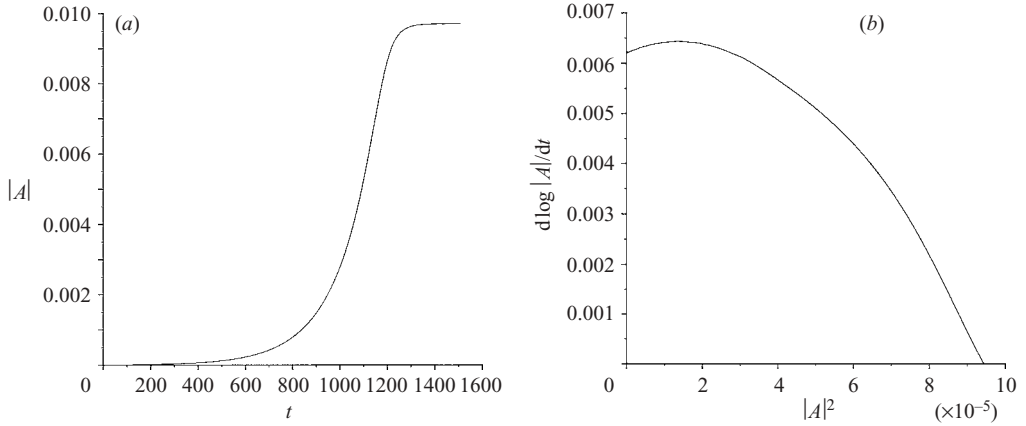
FIGURE 24. (*a*) The growth and saturation of the envelope of the non-axisymmetric transient corresponding to the Mode A instability of a ring with aspect ratio $Ar = 10$ at $Re = 200$. (*b*) The derivative of the amplitude logarithm against the square of the amplitude, which indicates subcritical behaviour.
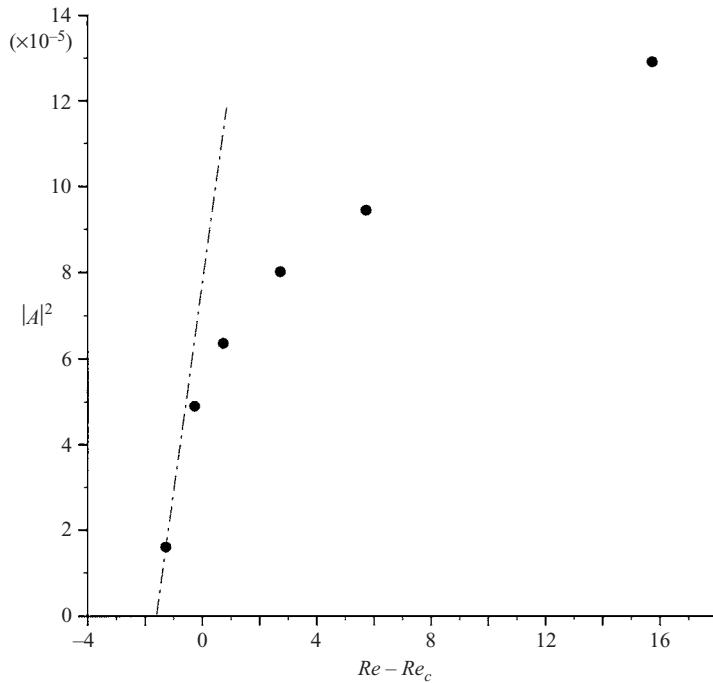

FIGURE 25. $|A|^2$ against $Re - Re_c$ for the Mode A instability in the flow past a ring with $Ar = 10$. $Re_c \approx 194.3$, and hysteretic behaviour is indicated.

6.2.3. *Secondary instabilities: wake structures and nonlinear transition properties*

The pure wakes of two instabilities were computed in the flow past a ring with $Ar = 10$. In figure 23(*b*), the wake which evolved from the Mode C instability at $Re = 230$ is shown, and in figure 23(*c*), the wake which evolved from a Mode B instability at $Re = 275$ is shown.

Similar to the Mode C wake in the flow past a ring with $Ar = 5$, the Mode C wake in the flow past a ring with $Ar = 10$ displays wake structures with an azimuthal wavelength of approximately $1.7d$ and a subharmonic spatio-temporal symmetry. Likewise, the structure of the Mode B wake in the flow past a ring with $Ar = 10$ is similar to the Mode B wake computed in the flow past a ring with $Ar = 5$, with an azimuthal wavelength of approximately $0.8d$.

An L_2 norm of the non-axisymmetry in the flows was monitored as the evolution of these instabilities was computed. In analysis, the Mode C transition was found to occur through a subcritical bifurcation, which was different to the supercritical behaviour computed for the Mode C instability in the flow past a ring with $Ar = 5$. However, the Mode B transition was found to occur through a supercritical bifurcation, as was the Mode B transition in the flow past a ring with $Ar = 5$.

For the nonlinear evolution of the Mode C instability, it is proposed that fifth-order terms are required in the Landau equation to describe the transition to saturation in the flow past rings, regardless of the sign of the cubic l–term, which changes sign at some aspect ratio in the range $5 < Ar < 10$. The physical mechanism responsible for the change in hysteretic behaviour with aspect ratio has not yet been determined, although it is likely to be associated with the change in the shedding angle of the vortex street.

6.3. *Wake instability mode path A–B–C: Ar = 20*

In this subsection iso-surface plots and the results of the application of the Landau model to the evolution of the non-axisymmetric modes in the flow past a ring with $Ar = 20$ are presented.

6.3.1. *Wake structure after the Mode A transition*

The saturated wake from the evolution of the Mode A instability for a ring with $Ar = 20$ is presented in figure 26(a). It may be observed that the mode has an azimuthal wavelength of approximately $4d$, which is similar to the Mode A wake in the flow past a ring with $Ar = 10$. The dye visualization experiments of Williamson (1988b) also show a similar wavelength for the Mode A wake behind a circular cylinder, as do the computations of Thompson *et al.* (1994, 1996) and Henderson (1997).

The periodicity of the Mode A wake is locked to the periodicity of the vortex street, and the spatio-temporal symmetry and streamwise vorticity distribution is similar to those described earlier for the Mode A wake in the flow past a ring with $Ar = 10$. The small curvature of a ring with $Ar = 20$ enhances the similarity between the Mode A wake presented here, and the Mode A wake observed behind a circular cylinder. A useful comparison may be made with the isosurface plots of the Mode A instability computed in the flow past a circular cylinder by Thompson *et al.* (1994, 1996) which employed a similar colour scheme.

6.3.2. *Application of the Landau model to the Mode A transition*

The evolution of the Mode A wake at $Re = 195$ for $Ar = 20$ is monitored to evaluate the coefficients of the Landau model. Figure 27(a) shows the growth and saturation of the Mode A amplitude, and figure 27(b) shows the nonlinear variation in growth rate with $|A|^2$ that is used to evaluate the pertinent coefficients of the Landau model.

The curve in figure 27(b) has a positive gradient in the vicinity of the y-axis, but over the range of $|A|^2$ is highly nonlinear. Thesecharacteristics suggest that at least
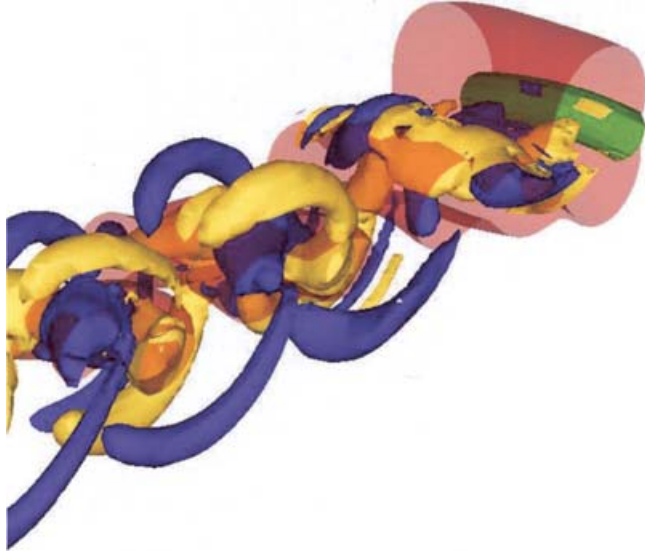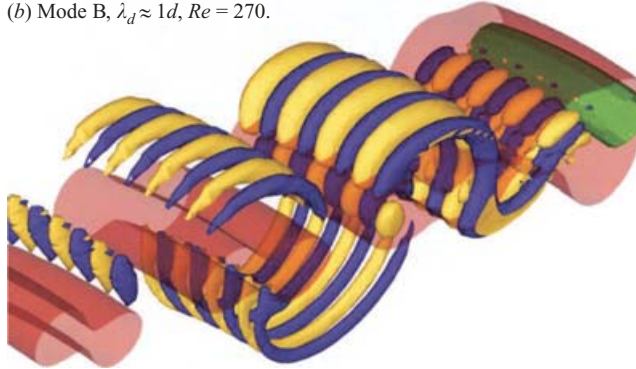
(*a*) Mode A, $\lambda_d \approx 4d$, $Re = 200$.

(*b*) Mode B, $\lambda_d \approx 1d$, $Re = 270$.

FIGURE 26. Isosurface plots showing the vortex structure of the non-axisymmetric flow past a ring with $Ar = 20$. Isosurface colours are as in figure 20.

fifth-order terms are necessary for the Landau model to describe the saturation, and that the transition occurs through a subcritical bifurcation.

A plot of $|A|^2$ against $Re - Re_c$ is presented in figure 28, which verifies that hysteresis is found at the onset of the Mode A transition, as the computed amplitude is non-zero at $Re - Re_c = 0$.

6.3.3. *The secondary instability: wake structure and nonlinear transition properties*

A plot which shows the structure of the computed wake which evolves from the Mode B instability in the flow past a ring with $Ar = 20$ is shown in figure 26(*b*). The plot shows that the wake has structural properties and spatio-temporal symmetry properties which are similar to both the Mode B wake computed in the flow past rings with $Ar = 5$ and 10, and the flow past a circular cylinder (Thompson *et al.* 1994, 1996).
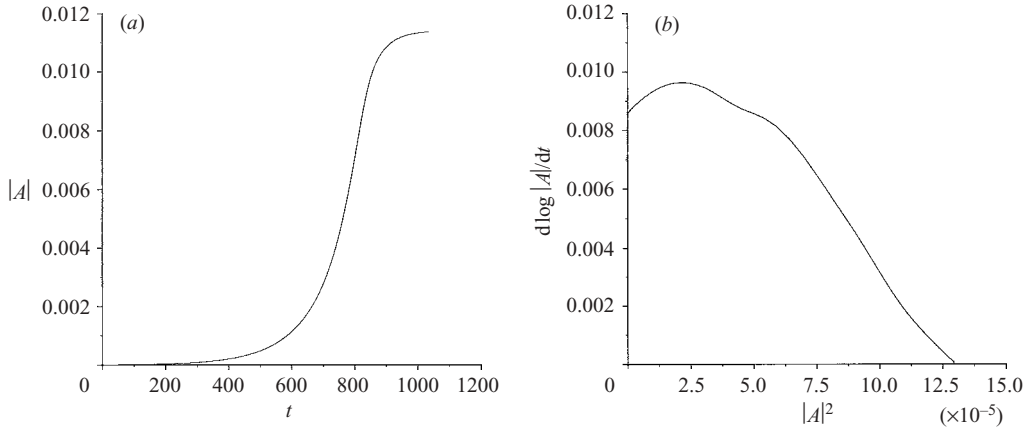
FIGURE 27. (*a*) The growth and saturation of the envelope of the non-axisymmetric transient corresponding to the Mode A instability of a ring with aspect ratio $Ar = 20$ at $Re = 195$. (*b*) The derivative of the amplitude logarithm against the square of the amplitude, which shows subcritical behaviour.
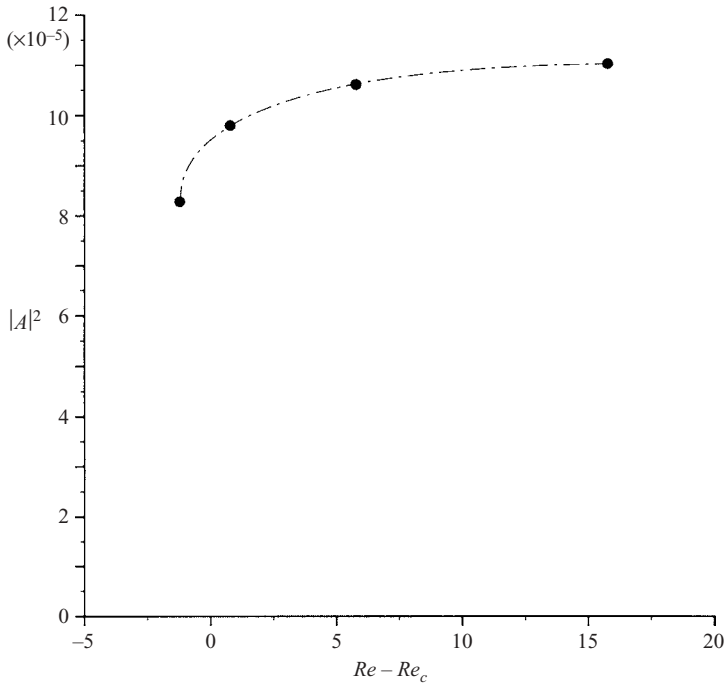

FIGURE 28. $|A|^2$ against $Re - Re_c$ for the pure Mode A instability in the flow past a ring with $Ar = 20$. $Re_c \approx 189.2$, and hysteretic behaviour is indicated.

An L_2 norm of the non-axisymmetry in the flow was monitored as the evolution of the Mode B instability was computed. In analysis, the Mode B transition was predicted to occur through a supercritical bifurcation. This predicted transition behaviour was again confirmed by computations at several Reynolds numbers in the vicinity of Re_c.

7. Conclusions

Isosurface plots have been presented showing the wake structures that occur following both the regular and Hopf transitions for tori with aspect ratios $Ar \lesssim 3.9$. The predictions from a previous stability analysis study pertaining to the presence of three distinct transition modes in the aspect ratio regime $0 \leqslant Ar \lesssim 3.9$ have been verified. The predicted transition Reynolds numbers have also been verified. These transitions are: a regular transition, Mode I, occurring in the aspect ratio range $0 \leqslant Ar < 1.6$; a Hopf transition, Mode II, occurring in the range $1.6 \leqslant Ar \leqslant 1.7$; and another regular transition, Mode III, occurring in the range $1.7 < Ar < 4$.

The Mode I transition is shown to be analogous to the regular transition of the sphere wake to a non-axisymmetric state, and is characterized by the classic 'double-threaded wake' observed for a sphere. The azimuthal symmetry of the Mode I transition is $m = 1$. Landau modelling has predicted that the regular Mode I transition is supercritical, consistent with the flow past a sphere. A supercritical Hopf transition is shown to develop following the regular Mode I transition. The azimuthal mode number of this instability is also $m = 1$, and the wake consists of hairpins or vortex loops being cast into the wake from alternate sides of the ring every half-period. This wake is almost identical in structure to the unsteady wake behind a sphere.

The Mode II transition is shown to lead to a very low-frequency non-periodic oscillating non-axisymmetric wake, again with azimuthal symmetry $m = 1$. Predictions that the mode evolves spontaneously to an unsteady non-axisymmetric wake due to the instability being a complex-conjugate Floquet mode are verified. Landau modelling verifies that the Mode II transition is also supercritical.

The regular Mode III wake is dominated by non-axisymmetric vortical structures in the near-wake region in the vicinity of the recirculation bubble behind the ring cross-section. The azimuthal symmetry of the Mode III transition is $m = 1$ for $Ar = 2$, and $m = 2$ for $Ar = 3$. The regular Mode III transition was found to be subcritical, showing strong bi-stability (hysteresis) at the onset of the transition. A secondary non-axisymmetric transition is found for the Mode III regime at higher Reynolds numbers. This Hopf transition is found to be supercritical, and structurally consists of vortex loops, consistent with the Hopf transitions in the Mode I and Mode II regimes. The azimuthal mode number of the Hopf mode in the Mode III regime follows the corresponding symmetry of the regular transition mode.

The pure non-axisymmetric instabilities that are predicted for the flow past rings with $Ar = 5$, 10 and 20 are computed. These aspect ratios are employed to study the three distinct transition paths with increasing Reynolds number, namely; Modes C–A–B for $Ar = 5$, Modes A–C–B for $Ar = 10$ and Modes A–B–C for $Ar = 20$. The Mode A instability in the flow past a ring with $Ar = 5$ and the Mode C instability in the flow past a ring with $Ar = 20$ were not computed as the growth of the instabilities was contaminated by the evolution of an earlier-occurring instability with a shorter azimuthal wavelength.

In the flow past a ring with $Ar = 5$, the first-occurring subharmonic Mode C instability produces a period-doubling in the wake. The transition is supercritical, with no hysteresis observed at the onset. In the flow past rings with $Ar = 10$ and 20, the first-occurring subharmonic Mode A instability evolves to wakes which are structurally analogous to the Mode A wake behind a circular cylinder. A region of hysteresis is computed at the onset of the instability.

The variation in the Landau constant (c) and the Landau diffusivity constant with aspect ratio are calculated for the primary Hopf transition for all aspect ratios. The primary Hopf transition was computed to be supercritical throughout the aspect ratio

range studied here, which suggests that no hysteresis will be found at the onset of unsteady flow.

The first-occurring non-axisymmetric instability has been shown to be supercritical for the ranges $0 \leqslant Ar < 1.8$ (Modes I and II) and $3.9 \lesssim Ar \lesssim 8$ (Mode C) and subcritical for the ranges $1.8 \lesssim Ar \lesssim 3.9$ (Mode III) and $Ar \gtrsim 8$ (Mode A). This means that the wakes observed for a majority of aspect ratios will exhibit some hysteresis in the vicinity of the transitions.

REFERENCES

BARKLEY, D. & HENDERSON, R. D. 1996 Three-dimensional Floquet stability analysis of the wake of a circular cylinder. *J. Fluid Mech.* **322**, 215–241.

BEARMAN, P. W. & TAKAMOTO, M. 1988 Vortex shedding behind rings and disks. *Fluid Dyn. Res.* **3**, 214.

BLACKBURN, H. M. & LOPEZ, J. M. 2003 On three-dimensional quasi-periodic Floquet instabilities of two-dimensional bluff body wakes. *Phys. Fluids* **15**, L57–L60.

DUŠEK, J., FRAUNIÉ, P. & LE GAL, P. 1994 A numerical and theoretical study of the first Hopf bifurcation in a cylinder wake. *J. Fluid Mech.* **264**, 59–80.

GHIDERSA, B. & DUŠEK, J. 2000 Breaking of axisymmetry and onset of unsteadiness in the wake of a sphere. *J. Fluid Mech.* **423**, 33–69.

HENDERSON, R. D. 1997 Nonlinear dynamics and pattern formation in turbulent wake transition. *J. Fluid Mech.* **352**, 65–112.

HOURIGAN, K., THOMPSON, M. C. & TAN, B. T. 2001 Self-sustained oscillations in flows around long flat plates. *J. Fluids Struct.* **15**, 387–398.

JEONG, J. & HUSSAIN, F. 1995 On the identification of a vortex. *J. Fluid Mech.* **285**, 69–94.

JOHNSON, T. A. & PATEL, V. C. 1999 Flow past a sphere up to a Reynolds number of 300. *J. Fluid Mech.* **378**, 19–70.

LANDAU, L. D. & LIFSHITZ, E. M. 1976 *Mechanics*, 3rd Edn. Pergamon.

LE GAL, P., NADIM, A. & THOMPSON, M. C. 2001 Hysteresis in the forced Stuart-Landau equation: Application to vortex shedding from an oscillating cylinder. *J. Fluids Struct.* **15**, 445–457.

LEWEKE, T. & PROVANSAL, M. 1995 The flow behind rings: Bluff body wakes without end effects. *J. Fluid Mech.* **288**, 265–310.

MAGARVEY, R. H. & BISHOP, R. L. 1961a Transition ranges for three-dimensional wakes. *Canadian J. Phys.* **39**, 1418–1422.

MAGARVEY, R. H. & BISHOP, R. L. 1961b Wakes in liquid-liquid systems. *Phys. Fluids* **4**, 800–805.

MAGARVEY, R. H. & MACLATCHY, C. S. 1965 Vortices in sphere wakes. *Canadian J. Phys.* **43**, 1649–1656.

MILLS, R., SHERIDAN, J. & HOURIGAN, K. 2002 Response of base suction and vortex shedding from rectangular prisms to transverse forcing. *J. Fluid Mech.* **461**, 25–49.

MILLS, R., SHERIDAN, J. & HOURIGAN, K. 2003 Particle image velocimetry and visualization of natural and forced flow around rectangular cylinders. *J. Fluid Mech.* **478**, 299–323.

MITTAL, R. 1999 A Fourier-Chebyshev spectral collocation method for simulating flow past spheres and spheroids. *Intl J. Numer. Fluids* **30**, 921–937.

MONSON, D. R. 1983 The effect of transverse curvature on the drag and vortex shedding of elongated bluff bodies at low Reynolds number. *Trans. ASME* I: *J. Fluids Engng* **105**, 308–317.

NATARAJAN, R. & ACRIVOS, A. 1993 The instability of the steady flow past spheres and disks. *J. Fluid Mech.* **254**, 323–344.

NOACK, B. R. & ECKELMANN, H. 1994 A low-dimensional Galerkin method for the three-dimensional flow around a circular cylinder. *Phys. Fluids* **6**, 124–143.

ORMIÈRES, D. & PROVANSAL, M. 1999 Transition to turbulence in the wake of a sphere. *Phys. Rev. Lett.* **83**, 80–83.

PROVANSAL, M., MATHIS, C. & BOYER, L. 1987 Bérnard-von kármán instability: Transient and forced regimes. *J. Fluid Mech.* **182**, 1–22.

PROVANSAL, M. & ORMIÈRES, D. 1998 Etudé expérimentale de l'instabilité du sillage d'une sphère. *C. R. Acad. Sci. Paris* **326** (II b), 489–498.

ROBICHAUX, J., BALACHANDAR, S. & VANKA, S. P. 1999 Three-dimensional Floquet instability of the wake of a square cylinder. *Phys. Fluids* **11**, 560–578.

ROSHKO, A. 1953 On the development of turbulent wakes from vortex streets. *NACA Tech. Note* p. 2913.

SHEARD, G. J., THOMPSON, M. C. & HOURIGAN, K. 2001 A numerical study of bluff ring wake stability. In *Proc. 14th Australasian Fluid Mechanics Conf. 9–14 December* (ed. B. B. Dally) Department of Mechanical Engineering, University of Adelaide.

SHEARD, G. J., THOMPSON, M. C. & HOURIGAN, K. 2002 On axisymmetric bluff body wakes: Three-dimensional wake structures and transition criticality of the torus. In *Proc. 3rd Conf. on Bluff Body Wakes and Vortex Induced Vibrations 17–20 December* (ed. K. Hourigan, T. Leweke, M. C. Thompson & C. H. K. Williamson). Port Douglas, Australia.

SHEARD, G. J., THOMPSON, M. C. & HOURIGAN, K. 2003 From spheres to circular cylinders: The stability and flow structures of bluff ring wakes. *J. Fluid Mech.* **492**, 147–180.

TANEDA, S. 1956 Experimental investigation of the wake behind a sphere at low Reynolds numbers. *J. Phys. Soc. Japan* **11**, 1104–1108.

THOMPSON, M. C., HOURIGAN, K. & SHERIDAN, J. 1994 Three-dimensional instabilities in the wake of a circular cylinder. In *Proc. Intl Colloq. on Jets, Wakes and Shear Layers, CSIRO, Division of Building Construction & Engineering, Highett, Australia*. CSIRO, Melbourne.

THOMPSON, M. C., HOURIGAN, K. & SHERIDAN, J. 1996 Three-dimensional instabilities in the wake of a circular cylinder. *Expl. Therm. Fluid Sci.* **12**, 190–196.

THOMPSON, M. C., LEWEKE, T. & PROVANSAL, M. 2001*a* Kinematics and dynamics of sphere wake transition. *J. Fluids Struct.* **15**, 575–585.

THOMPSON, M. C., LEWEKE, T. & WILLIAMSON, C. H. K. 2001*b* The physical mechanism of transition in bluff body wakes. *J. Fluids Struct.* **15**, 607–616.

TOMBOULIDES, A. G. & ORSZAG, S. A. 2000 Numerical investigation of transitional and weak turbulent flow past a sphere. *J. Fluid Mech.* **416**, 45–73.

WILLIAMSON, C. H. K. 1988*a* Defining a universal and continuous Strouhal-Reynolds number relationship for the laminar vortex shedding of a circular cylinder. *Phys. Fluids* **31**, 2742–2744.

WILLIAMSON, C. H. K. 1988*b* The existence of two stages in the transition to three-dimensionality of a cylinder wake. *Phys. Fluids* **31**, 3165–3168.

WILLIAMSON, C. H. K. 1989 Oblique and parallel mode of vortex shedding in the wake of a circular cylinder at low Reynolds numbers. *J. Fluid Mech.* **206**, 579–627.

WILLIAMSON, C. H. K. 1996 Three-dimensional wake transition. *J. Fluid Mech.* **328**, 345–407.

WU, J., SHERIDAN, J., WELSH, M. & HOURIGAN, K. 1996 Three-dimensional vortex structures in a cylinder wake. *J. Fluid Mech.* **312**, 201–222.

ZHANG, H., NOACK, B. R., KÖNIG, M. & ECKELMANN, H. 1995 On the transition of the circular cylinder wake. *Phys. Fluids* **7**, 779–793.

ZIELINSKA, B. J. A. & WESFREID, J. E. 1995 On the spatial structure of global modes in wake flows. *Phys. Fluids* **7**, 1418–1424.